

# 1 **Archaeal Intact Polar Lipids in Polar Waters: A Comparison Between** 2 **the Amundsen and Scotia Seas**

3 Charlotte L. Spencer-Jones<sup>1</sup>, Erin L. McClymont<sup>1</sup>, Nicole J. Bale<sup>2</sup>, Ellen C. Hopmans<sup>2</sup>,  
4 Stefan Schouten<sup>2,3</sup>, Juliane Müller<sup>4</sup>, E. Povl Abrahamsen<sup>5</sup>, Claire Allen<sup>5</sup>, Torsten  
5 Bickert<sup>4</sup>, Claus-Dieter Hillenbrand<sup>5</sup>, Elaine Mawbey<sup>5</sup>, Victoria Peck<sup>5</sup>, Aleksandra  
6 Svalova<sup>6</sup>, James A. Smith<sup>5</sup>

7 <sup>1</sup>Department of Geography, Durham University, Lower Mountjoy, South Road, Durham, DH1 3LE, UK.

8 <sup>2</sup>NIOZ Royal Netherlands Institute for Sea Research, Department of Marine Microbiology and  
9 Biogeochemistry, P.O. Box 59, 1790 AB Den Burg, Texel, The Netherlands.

10 <sup>3</sup> Department of Earth Sciences, Utrecht University, Utrecht, The Netherlands.

11 <sup>4</sup>Alfred Wegener Institute, Helmholtz Center for Polar and Marine Research, 27568 Bremerhaven, Germany.

12 <sup>5</sup>British Antarctic Survey, High Cross, Madingley Road, Cambridge, CB3 0ET, UK.

13 <sup>6</sup> School of Natural and Environmental Sciences, Newcastle University, Newcastle-upon-Tyne, NE1 7RU,  
14 UK.

15 Correspondence to: Charlotte L. Spencer-Jones ([charlotte.spencer-jones@open.ac.uk](mailto:charlotte.spencer-jones@open.ac.uk))

16 Abstract

17 The West Antarctic Ice Sheet (WAIS) is one of the largest potential sources of future sea-level rise, with  
18 glaciers draining the WAIS thinning at an accelerating rate over the past 40 years. Due to complexities in  
19 calibrating palaeoceanographic proxies for the Southern Ocean, it remains difficult to assess whether similar  
20 changes have occurred earlier during the Holocene or whether there is underlying centennial to millennial  
21 scale forcing in oceanic variability. Archaeal lipid – based proxies, specifically Glycerol Dialkyl Glycerol  
22 Tetraether (GDGT; e.g. TEX<sub>86</sub> and TEX<sub>86</sub><sup>L</sup>) are powerful tools for reconstructing ocean temperature, but  
23 these proxies have been shown previously to be difficult to apply to the Southern Ocean. A greater  
24 understanding of the parameters that control Southern Ocean GDGT distributions would improve the  
25 application of these biomarker proxies and thus help provide a longer-term perspective on ocean forcing of  
26 Antarctic ice sheet changes. In this study, we characterised intact polar lipid (IPL) - GDGTs, representing  
27 (recently) living archaeal populations in suspended particulate matter (SPM) from the Amundsen Sea and the  
28 Scotia Sea. SPM samples from the Amundsen Sea were collected from up to 4 water column depths  
29 representing the surface waters through to Circumpolar Deep Water (CDW) whereas the Scotia Sea samples  
30 were collected along a transect encompassing the sub-Antarctic front through to the southern boundary of the  
31 Antarctic Circumpolar Current. IPL-GDGTs with low cyclic diversity were detected throughout the water  
32 column with high relative abundances of hydroxylated IPL-GDGTs identified in both the Amundsen and

33 Scotia Seas. Results from the Scotia Sea show shifts in IPL-GDGT signatures across well-defined fronts of  
34 the Southern Ocean. Indicating that the physicochemical parameters of these water masses determine  
35 changes in IPL-GDGT distributions. The Amundsen Sea results identified GDGTs with hexose-  
36 phosphohexose head groups in the CDW suggesting active GDGT synthesis at these depths. These results  
37 suggest that GDGTs synthesized at CDW depths may be a significant source of GDGTs exported to the  
38 sedimentary record and that temperature reconstructions based on  $\text{TEX}_{86}$  or  $\text{TEX}_{86}^L$  proxies may be  
39 significantly influenced by the warmer waters of the CDW.

40 Key words

41 Southern Ocean, Intact Polar Lipid (IPL), Glycerol Dialkyl Glycerol Tetraether (GDGT), Amundsen Sea,  
42 Scotia Sea, Circumpolar Deep Water, Archaea, Thaumarchaeota.

### 43 **1. Introduction**

44 Over the past ca. 50 years the West Antarctic Ice Sheet (WAIS) has lost ice mass at an accelerating rate with  
45 some suggesting that the complete collapse of the WAIS may already be underway (Joughin et al., 2014;  
46 Mougnot et al., 2014; Rignot et al., 2019). The WAIS is grounded below sea level and the edges of the ice  
47 sheet are floating ice shelves that are, highly sensitive to changes in ocean properties. Widespread ice  
48 sheet/shelf thinning will likely have influence on biogeochemical cycling through ocean productivity  
49 (Raiswell et al., 2008; Menviel et al., 2010; Wadham et al., 2013), carbon reservoirs and carbon  
50 sequestration (Yager et al., 2012; Wadham et al., 2019), in addition to sea ice and ocean circulation changes  
51 (Menivel et al., 2010).

52 One of the challenges in understanding and predicting the behaviour of WAIS is a lack of long-term ocean  
53 temperature records (i.e. prior to the satellite era ~1992). Such records are needed to better understand the  
54 links between WAIS stability, physical properties of the Southern Ocean, and biogeochemistry which might  
55 vary on centennial to millennial timescales (Smith et al., 2017; Hillenbrand et al., 2017). Organic  
56 geochemical proxies based on the ratios of archaeal membrane lipids can be used to reconstruct past ocean  
57 temperature and biogeochemistry. Glycerol dialkyl glycerol tetraether (GDGT) lipids are particularly  
58 promising with the  $\text{TEX}_{86}$ ,  $\text{TEX}_{86}^L$  and OH-GDGT proxies having been widely used to reconstruct ocean  
59 temperatures in tropical, temperate, and northern polar regions (e.g. Jenkyns et al., 2004; Huguet et al., 2006,  
60 2011; Sinninghe Damsté et al., 2010; Darfeuil et al., 2016). In contrast, only a handful of studies have

61 successfully applied these proxies in the Southern Ocean (Kim et al., 2012; Shevenell et al., 2011; Etourneau  
62 et al., 2013, 2019). This reflects a combination of low concentrations of GDGTs with an incomplete  
63 understanding of archaeal populations and habitat/niche preference (Kim et al., 2010). A better  
64 understanding of the source of GDGTs in the Southern Ocean and factors that impact archaeal populations  
65 could improve application of TEX<sub>86</sub> based proxies in this environment.

### 66 **1.1. Tracing Archaea with Intact Polar Lipids**

67 Archaea are a key component of picoplankton within the polar oceans (DeLong et al., 1994; Murray et al.,  
68 1998; Church et al., 2003; Kirchman et al., 2007; Alonso-Saez et al., 2008) and have an important role in  
69 biogeochemical cycling and in marine food webs. GDGTs are important cell membrane components present  
70 in many marine archaea (Schouten et al., 2013 and references therein) including the ammonia oxidising  
71 archaea (AOA) Thaumarchaeota (previously assigned to the phylum Crenarchaeota; Brochier-Armanet et al.,  
72 2008; Spang et al., 2010). Marine archaea produce isoprenoid GDGTs with a polar head group (intact polar  
73 lipids - IPLs). Upon cell death the polar head group is relatively rapidly cleaved off resulting in the  
74 preservation of the core GDGT lipid (c-GDGTs). c-GDGTs are subsequently preserved in the sedimentary  
75 record and can be used to reconstruct Antarctic palaeoenvironmental change over long time scales (Kim et  
76 al., 2012; Shevenell et al., 2011; Etourneau et al., 2013, 2019). Thaumarchaeota are a major source of  
77 GDGTs to the environment with pure culture studies detecting GDGTs with 0-3 cyclopentane moieties,  
78 crenarchaeol (cren, which contains 4 cyclopentane moieties and a cyclohexane moiety) and cren regio isomer  
79 (cren', Schouten et al., 2000; Sinninghe Damsté et al., 2018). Other archaeal phyla (e.g. marine  
80 Euryarchaeota group II) have been hypothesised as sources of GDGTs to the marine realm (Lincoln et al.,  
81 2014a,b), however this source is unlikely to be significant in marine samples (Schouten et al., 2014; Zeng et  
82 al., 2019; Besseling et al., 2020). Furthermore, archaea exist throughout the marine water column with  
83 several studies suggesting a GDGT contribution to sediments from “deep water” Thaumarchaeota (e.g. Ingalls  
84 et al., 2006; Shah et al., 2008; Kim et al., 2016).

85 IPL-GDGTs may be used as proxies for tracing (recently) living archaeal populations (e.g. Pitcher et al.,  
86 2011; Sinninghe Damsté et al., 2012; Elling et al., 2014, 2017). AOA enrichment cultures reveal three  
87 common GDGT head groups; monohexose (MH), dihexose (DH), and hexose-phosphohexose (HPH)  
88 (Schouten et al., 2008; Pitcher et al., 2010, 2011), with all three IPL head groups reported in environmental

89 samples (Lipp et al., 2008; Lipp and Hinrichs, 2009; Schubotz et al., 2009; Schouten et al., 2012; Xie et al.,  
90 2014; Evans et al., 2017; Sollich et al., 2017; Besseling et al., 2018). HPHs are a common IPL in all AOA  
91 enrichment cultures, to date, with MH and DH intermittently present (Pitcher et al., 2011; Elling et al., 2017;  
92 Bale et al., 2019). The interpretation of IPL-GDGTs as proxies for living archaeal biomass is complicated by  
93 their degradation to c-GDGTs with increasing evidence that some IPLs are preserved following cell death  
94 (Bauersachs et al., 2010; Huguet et al., 2010; Schouten et al., 2010; Xie et al., 2013; Lengger et al., 2014).  
95 Kinetic modelling has suggested greater preservation of glycolipids compared with phospholipids (Schouten  
96 et al., 2010), therefore suggesting that HPH-GDGTs may have potential as biomarkers for living,  
97 metabolically active, Thaumarchaeotal populations (Schouten et al., 2012; Elling et al., 2014, 2017).  
98 However, HPH-GDGT abundance is variable across the 1.1a Thaumarchaeota clade which could make the  
99 interpretation of this biomarker in environmental studies complex (Elling et al., 2017). DH-GDGTs and DH-  
100 OH-GDGT on the other hand are thought to be produced exclusively by 1.1a Thaumarchaeota with more  
101 uniform abundance across the clade (Pitcher et al., 2011; Sinninghe Damsté et al., 2012), and could therefore  
102 be potential tracers for living Thaumarchaeota (Elling et al., 2017).  
103 In this study, we present the first characterisation of IPL-GDGTs in suspended particulate matter (SPM)  
104 from two locations in the Southern Ocean, the Scotia Sea and the Amundsen Sea. The first aim of this study  
105 is to characterise the distributions of IPL-GDGTs within the Southern Ocean in order to expand our  
106 understanding of Thaumarchaeotal distributions in Polar Regions and improve our interpretation of GDGT  
107 based proxies. The second aim of this study is to understand the environmental controls on IPL-GDGT  
108 distributions in the Southern Ocean. In this study, we analyse the water column profiles of IPL-GDGTs with  
109 18 samples from the Amundsen Sea and 30 samples from a transect in the Scotia and Weddell Sea.

## 110 **2. Methodology**

### 111 **2.1. Study Area**

112 The Southern Ocean drives the global thermohaline circulation and is therefore a major regulator of Earth's  
113 oceans and climate (Carter et al., 2009). The eastward flowing Antarctic Circumpolar Current (ACC)  
114 connects all the major ocean basins resulting in a major role in the distribution of heat, salt, and gasses  
115 (Carter et al., 2009). The surface waters of the Southern Ocean show clear shifts in water properties (salinity  
116 and temperature) which mark ocean fronts, and in the present study include the: Sub-Antarctic Front (SAF),

117 the Polar Front (PF), the Southern Front of the ACC (SACCF), and the Southern Boundary of the ACC  
118 (SBACC) (Carter et al., 2009 and references therein). Antarctic surface waters (AASW; 100m thick),  
119 extending from the Antarctic continental shelf to the PF, are characterised by near freezing temperatures and  
120 salinity values up to 34.3 practical salinity units (PSU), although these properties can vary on a regional basis  
121 (Carter et al., 2009 and references therein). The transition between AASW south of the PF and Sub-Antarctic  
122 surface water (SASW) north of the SAF occurs in the Polar Frontal Zone. Due to complex mixing processes,  
123 the properties of surface water in the Polar Frontal Zone are often variable, but this water is generally  
124 warmer (3-8 °C) and less dense (salinity 34-34.4 PSU) than AASW (Carter et al., 2009 and references  
125 therein). Lastly, SASW is comparatively warmer (6-12 °C) with salinity >34.3 PSU (Carter et al., 2009 and  
126 references therein). Circumpolar Deep Water (CDW) together with CDW-derived, modified deep-water  
127 masses, such as Warm Deep Water in the Weddell Gyre (e.g. Vernet et al., 2019) is a key Southern Ocean  
128 water mass and can be detected between ~1400 m and >3500 m depth offshore from the Antarctic continent.  
129 CDW can rise to meet AASW or even outcrop along the Antarctic continental margin (Carter et al., 2009 and  
130 references therein). Mixing of CDW with different water masses gives rise to two types: Upper CDW  
131 (UCDW) defined by an oxygen minimum, high nutrient concentrations, and a depth of 1400-2500 m; and  
132 Lower CDW (LCDW) defined by a salinity maximum of 34.70-34.75 PSU (Carter et al., 2009 and  
133 references therein). In contrast to UCDW, LCDW extends south of the SBACC (Orsi et al., 1995), is  
134 upwelled at the continental slope, and can protrude onto the shelf where it mixes with shelf waters cooled by  
135 interactions with the ice shelves and atmosphere (sometimes below the surface freezing point), renewing  
136 LCDW and forming Antarctic Bottom Water (AABW) (Carter et al., 2009 and references therein).

137 The Scotia Sea is located in the eastern Atlantic sector of the Southern Ocean (20°W to 65°W) bounded by  
138 the South Atlantic Ocean to the North, the Drake Passage to the West, and by the Weddell Sea to the South  
139 (Figure 1). The Scotia Sea is influenced by the eastward flow of the ACC, via the Drake Passage, and by a  
140 northward component of the ACC, caused by topographic steering and northward outflow of recently  
141 ventilated waters from the Weddell Sea, whereby Weddell Sea Deep Water (WSDW) is incorporated into  
142 the ACC (Locarnini et al., 1993; Naveira Garabato et al., 2002a,b), thus creating a region of high mixing  
143 (Heywood et al., 2002) and intense water mass modification (Locarnini et al., 1993).

144 The Amundsen Sea extends from 100°W to 130°W and is bounded by the Sub-Antarctic Pacific to the North  
145 (Figure 1). The Amundsen Sea water column south of the PF mainly consist of a thin upper layer of cold and  
146 fresh AASW overlying relatively warm CDW. The Amundsen Sea Embayment is located offshore from one  
147 of the major WAIS drainage basins and observations show a clear trend in glacial retreat over recent decades  
148 (e.g. Mouginot et al., 2014; Paolo et al., 2015; Rignot et al., 2019). The deep ice shelves (extending up to  
149 1000 m below sea level) surrounding the Amundsen Sea embayment are exposed to unmodified CDW which  
150 can be up to 4 °C above the *in situ* freezing point (Jacobs et al., 1996, 2011; Rignot and Jacobs, 2002;  
151 Jenkins et al., 2010; Rignot et al., 2013; Webber et al., 2017) so that CDW may drive enhanced melt rates  
152 and ice sheet instability in this region (Shepherd et al., 2001; Zwally et al., 2005; Rignot et al., 2008;  
153 Pritchard et al., 2009; Wingham et al., 2009).

## 154 **2.2. Sample collection**

155 A Seabird Scientific SBE911plus conductivity-temperature-depth (CTD) instrument with a 24 bottle rosette  
156 was used to vertically profile the water column and collect water for organic geochemical analysis. Water  
157 was collected on board the RRS *James Clark Ross* (expeditions JR272 and JR257) during March-April 2012  
158 (austral autumn) from 15 stations along the former WOCE A23 section (Meredith et al., 2001) traversing the  
159 Scotia Sea between the northern Weddell Sea and South Georgia (Table 1 and Figure 1; Allen et al., 2012;  
160 Venables et al., 2012), and on board the R/V *Polarstern* expedition PS104 during February-March 2017  
161 (austral summer) from 5 stations in the Amundsen Sea embayment (Table 2 and Figure 1; Gohl, 2017).  
162 Water samples were collected in 10 L Niskin bottles. In the Scotia Sea, the depth of the sample collection  
163 was dependent on the expression of the mixed layer and seasonal thermocline as observed during each CTD  
164 deployment. At all stations, a “mixed layer” sample was collected between 10-40m depth and a “thermocline  
165 layer” sample collected between approximately 60-110 m depth (Table 1). In the Amundsen Sea, the  
166 sampling strategy included samples from surface thermocline waters, and CDW. Water samples  
167 (approximately 10-30 L) were vacuum filtered through pre-combusted GF/F filters (Whatman, 0.7 µm pore  
168 size, 50 mm diameter). Glass fibre filters with a nominal pore size of 0.7 µm are most commonly used for  
169 sampling of SPM in ocean and lake waters. However, as microbes can range in size from 0.2-0.7 µm, these  
170 filters may lead to an under-sampling of archaeal cells that are not associated with aggregates (Lee et al.,

171 1995; Ingalls et al., 2012). Therefore, IPL-GDGT concentrations reported here represent the minimum likely  
172 concentrations.

173 The filters were subsequently stored in foil at -20 °C, then transported to Durham University (UK; Scotia sea  
174 samples) and Alfred Wegener Institute (Germany; Amundsen Sea samples). Samples were freeze-dried prior  
175 to lipid extraction.

### 176 **2.3. Sample extraction**

177 Total lipids of the Scotia Sea sample set were extracted at the Royal Netherlands Institute for Sea Research.  
178 Freeze-dried samples were extracted using a modified Bligh and Dyer methodology as detailed in Besseling  
179 et al. (2018). Briefly, sample filters were cut into small pieces using solvent cleaned scissors. The total lipids  
180 were extracted using a monophasic mixture of K<sub>2</sub>HPO<sub>4</sub> (8 g/L adjusted to pH 7-8), dichloromethane  
181 (CH<sub>2</sub>Cl<sub>2</sub>) and methanol (CH<sub>3</sub>OH) at a ratio of 0.8:1:2. Extractions were repeated three times and pooled. The  
182 pooled extract was subsequently phase separated by adjusting the ratio of K<sub>2</sub>HPO<sub>4</sub>: CH<sub>2</sub>Cl<sub>2</sub>: CH<sub>3</sub>OH to  
183 0.9:1:1. The CH<sub>2</sub>Cl<sub>2</sub> layer of the resultant bi-phasic mixture was transferred to a round bottom flask. This  
184 was repeated three times, with the Bligh Dyer extract dried under a stream of N<sub>2</sub>.

185 Total lipids of the Amundsen Sea sample set were extracted at the Alfred Wegener Institute (Germany).  
186 Freeze dried samples were extracted ultrasonically using CH<sub>2</sub>Cl<sub>2</sub> and CH<sub>3</sub>OH at a ratio of 2:1 for 15 minutes.  
187 This was repeated three times, the extracts pooled and dried under a stream of N<sub>2</sub>. The resulting total lipid  
188 extract was fractionated over a silica column using hexane (for elution of the alkanes and highly branched  
189 isoprenoids) followed by CH<sub>2</sub>Cl<sub>2</sub>:hexane and CH<sub>2</sub>Cl<sub>2</sub>:CH<sub>3</sub>OH both at a ratio of 1:1 for elution of the polar  
190 fraction. The polar fraction was dried under N<sub>2</sub> and stored at -20 °C prior to IPL-GDGT analysis. The  
191 method used for the extraction of the Amundsen Sea samples is not the Bligh Dyer protocol most commonly  
192 used for IPL-GDGT extraction. Extraction technique has not been found to significantly affect c-GDGTs  
193 recovery (Schouten et al., 2013; Weber et al., 2017) but has been found to have a greater influence on IPL-  
194 GDGT recovery due to differences in polar moieties (Weber et al., 2017). Weber et al. (2017) found  
195 extraction procedure to impact the absolute quantification of GDGTs along with the recovery of cren'  
196 (under-quantified) and GDGT-3 (over-quantified). Sample purification using silica gel column  
197 chromatography has also been found to have an impact on IPL-GDGT recovery (Pitcher et al., 2009;  
198 Lengger et al., 2012) with HPH-GDGTs under-quantified (Lengger et al., 2012). We acknowledge that there

199 may be some differences in IPL-GDGT recovery between the Amundsen and Scotia sea samples due to  
200 differences in extraction and work-up technique. However, we propose that comparison can still be made  
201 between the two seas as we do not report absolute quantities of IPL-GDGTs as the methods are semi-  
202 quantitative, we do not report the occurrence of cren', and GDGT-3 was below the detection limit of the  
203 instrument. An internal standard of 1-O-hexadecyl-2-acetyl-*sn*-glycero-3-phosphocholine was added to both  
204 the Amundsen and Scotia Sea samples. The Bligh Dyer extract (Scotia Sea) and polar fraction (Amundsen  
205 Sea) were filtered through true regenerated cellulose filters (4 mm, 0.45 µm pore size) using hexane, propan-  
206 2-ol, and water at a ratio of 79:20:1. Samples were stored at -20 °C prior to analysis.

#### 207 **2.4. Intact Polar Lipid characterisation**

208 IPL-GDGTs were analysed using a modification of the Sturt et al. (2004) methodology as detailed in  
209 Besseling et al. (2018). To summarise, an Agilent 1290 Infinity I UHPLC, equipped with a thermostated  
210 auto-injector and column oven, coupled to a Q Exactive Orbitrap MS with Ion Max source with a heated  
211 electrospray ionisation (HESI) probe (Thermo Fisher Scientific, Waltham, MA, USA). Separation was  
212 achieved using a YMC-Triart Diol-HILIC column (250 x 2.0 mm, 1.9 µm particle size, 12 nm pore size;  
213 YMC co., Ltd., Kyoto, Japan) maintained at 30 °C with a flow rate of 0.2 mL/min. Chromatographic  
214 separation of IPL-GDGTs was achieved using the following 70 minute program: 0% eluent B from 0-5  
215 minutes, linear gradient to 34% eluent B at 25 minutes, isocratic 25-40 minutes, linear gradient to 60% B at  
216 55 minutes, linear gradient to 70% B 65 minutes, followed by a re-equilibration time of 20 minutes between  
217 each analysis. Eluent A was hexane/propan-2-ol/formic acid/ 14.8 M NH<sub>3aq</sub> (79:20:0.12:0.04 [v/v/v/v]),  
218 eluent B is propan-2-ol/water/formic acid/14.8 M NH<sub>3aq</sub> (88:10:0.12:0.04 [v/v/v/v]). HESI sheath gas,  
219 auxiliary gas and sweep gas N<sub>2</sub> pressures were 35, 10, and 10 (arbitrary units) respectively with the auxiliary  
220 gas at 50 °C. The spray voltage was 4.0 kV (positive ion ESI), S-Lens 70 V, and capillary temperature 275  
221 °C. Mass range monitored was between *m/z* 375 and 2000 (resolving power of 70 000 ppm at *m/z* 200)  
222 followed by data dependent fragmentation of the 10 most abundant masses in the mass spectrum (with the  
223 exclusion of isotope peaks) were fragmented successively (stepped normalised collision energy 15, 22.5, 30;  
224 isolation window 1.0 *m/z*). A dynamic exclusion window of 6 s was used as well as an inclusion list with a  
225 mass tolerance of 3 ppm to target specific compounds (absolute *m/z* values of IPL-GDGTs can be found in  
226 supplement A and structures are found in supplement B S1). The Q Exactive Orbitrap MS was calibrated



227 within a mass accuracy range of 1 ppm using the Thermo Scientific Pierce LTQ Velos ESI Positive Ion  
228 Calibration Solution (containing a mixture of caffeine, MRFA, Ultramark 1621, and N-butylamine in an  
229 acetonitrile-methanol-acetic acid solution). Peak areas for each individual IPL were determined by  
230 integrating the combined mass chromatograms (within 3 ppm) of the monoisotopic and first isotope peak of  
231 all the relevant adducts formed (protonated, ammoniated, and/or sodiated). IPL-GDGTs were examined in  
232 terms of their MS peak area response. Thus, the relative abundance of the peak area does not necessarily  
233 reflect the actual relative abundance of the different IPL-GDGTs, however, this method allows for the  
234 comparison between samples analysed in this study. The peak areas were determined from extracted ion  
235 chromatograms of the  $[M+H]^+$ ,  $[M+NH_4]^+$ , and  $[M+Na]^+$  for each individual IPL-GDGT species. C-GDGT  
236 lipids were not analysed.

## 237 **2.5. Data Analysis**

238 Standards for individual IPL-GDGTs are not available and therefore concentrations reported here are semi-  
239 quantitative. IPL-GDGT peak areas were normalised to the internal standard and volume of water filtered  
240 and are reported as units/L. The Ring Index (RI) was calculated based on Zhang et al. (2016).  
241 Redundancy analysis (RDA) was performed on the Scotia Sea data set in RStudio (version 1.2.1335) using  
242 Vegan and Faraway packages. RDA was performed using data normalised to the internal standard and total  
243 water volume extracted (scaled). Temperature, salinity, oxygen concentration, and Chlorophyll *a*  
244 fluorescence (hereafter referred to as fluorescence) were selected as explanatory variables and IPL-GDGT  
245 relative abundances are the response variables. Statistical significance of RDA, axes, and explanatory  
246 variables were determined using an Anova-like test (Legendre et al., 2011).

## 247 **3. Results**

### 248 **3.1. Physicochemical properties of the water column**

249 CTD measurements were taken at all 5 stations in the Amundsen Sea: PS104/003, PS104/007, PS104/017,  
250 PS104/022, PS104/043. Temperature – salinity (T-S) plots are shown in Figure 2 and supplement B S2. At  
251 the time of sampling, water masses in the Amundsen Sea study area were characterised by a temperature  
252 range of -1.7 to +1.1 °C, a salinity range of 32.8 to 34.7 PSU, and a dissolved oxygen concentration of  
253 between 183.9 and 386.2  $\mu\text{mol/kg}$ . Three different water masses are detected in the Amundsen Sea from the

254 T-S plot: AASW, CDW, and modified CDW (Figure 2). Fluorescence peaked at the surface within the  
255 uppermost 20 m, followed by a steep decline with depth (Supplement B S2). High fluorescence values were  
256 observed at PS104/017 with 8mg/m<sup>3</sup>, and PS104/007 with 4 mg/m<sup>3</sup> respectively, whereas low fluorescence  
257 values were observed at stations PS104/003, PS104/022, and PS104/043 (Supplement B S2).

258 The Scotia Sea study area encompasses the SAF, PF, SACCF and the SBACC (Figure 1a) and is  
259 characterised by a temperature range of -1.6 to +7.3 °C, and a salinity range of 33.6-34.7 PSU (Figure 2).

260 The temperature range of the mixed layer samples was -1.2 to +7.3 °C and thermocline samples was -1.6 to  
261 +6.1 °C. A clear partition between the sample stations is observed in the T-S plot (Figure 2) with consistently  
262 higher water temperatures found at stations north of CTD 19 and on average lower ocean temperatures south  
263 of CTD 18. This region broadly marks the location of the SBACC at ~58.6 °S (Figure 1a).

### 264 **3.2. Amundsen Sea depth profiles**

265 Archaeal IPLs were identified in the water column at all Amundsen Sea stations (Table 3, Figure 3). The  
266 relative abundance of the regular GDGT core (i.e. non-hydroxylated) varied with depth ranging from 20-  
267 100% of total IPL-GDGTs (excluding depths where no IPL-GDGTs were identified; Table 3). PS104/003  
268 and PS104/007 were found to have IPL-GDGTs in the uppermost surface sample (10 m and 20 m depths  
269 respectively). The surface sample at PS104/003 (10m) was dominated by non-hydroxylated GDGTs (94.3%  
270 of total IPLs) with a lower relative abundance of OH-GDGT core type (5.7% of total IPLs). Further to this,  
271 HPH-GDGT-0 was the most abundant IPL-GDGT at this station (81.8% of total IPLs) with HPH-cren  
272 contributing a smaller fraction of the total IPL-GDGTs (11.1%). Low relative abundance of MH-GDGT-0  
273 (<1%), MH-cren (<1%), MH-OH-GDGT-0 (<1%), DH-OH-GDGT-0 (5.1%), and MH-diOH-GDGT-0  
274 (<1%) were also observed at PS104/003 10 m. This contrasts with the surface sample at PS104/007 (20 m)  
275 where no OH-GDGT-IPLs were detected and where the IPL-GDGT suite is split between MH-GDGT-0  
276 (89.1%) and MH-cren (10.9%). IPL-GDGTs were not identified within the surface sample at PS104/017 (10  
277 m) and the two mid-shelf stations, PS104/022 (10 m and 30 m) and PS104/043 (10 m). DH-GDGT-0 and  
278 DH-cren are minor components of the IPL-GDGT suite with maximum relative abundance observed in the  
279 deepest samples for all Amundsen Sea stations. The relative abundance of IPL-GDGTs with a MH head  
280 group peaks in the mid depths between 120 and 240 m (with the exception of the surface 20 m at  
281 PS104/007). The ratio of GDGT-0/cren is variable throughout the Amundsen Sea stations, ranging from 2.8-

282 8.2 (excluding samples with no GDGTs). The sample taken from 180 m water depth at PS104/003 exceeded  
283 this range with a GDGT-0/cren ratio of 27.0 (Table 2).

### 284 **3.3. Scotia Sea transect**

285 Archaeal IPLs were detected within all 16 Scotia Sea stations. A clear depth trend in IPL-GDGTs can be  
286 observed where IPL-GDGTs were detected in the thermocline samples but were often below detection within  
287 the mixed layer (Table 4 and Figure 4b). Exceptions to this are CTD 1, 16, 20, and 21 where IPL-GDGTs  
288 were present in both the mixed and thermocline layers. Relative abundance (%) of IPL-GDGT cores and the  
289 degree of cyclicity remains constant along the Scotia Sea transect with IPL-GDGT head groups showing  
290 greater variation along the transect (Table 4). An increase in the relative abundance of the HPH head group is  
291 observed within the thermocline samples between CTD 22 (53.5 °S) and 5 (63.3 °S) this is coupled with a  
292 decrease in the relative abundance (%) of MH and DH IPL-GDGT head groups (Figure 4b). Mixed layer  
293 CTD 20 and 21 are dominated by MH, CTD 16 is dominated by HPH, and CTD 1 mixed layer contains a  
294 mixture of all three IPL-GDGT head groups. The GDGT-0/cren ratio generally ranges from 1.6-9.9, but CTD  
295 7 (21.7), 10 (177.6), and 16 (16.8), located at the thermocline, exceed this range due to low cren  
296 concentrations (Table 1). In preparation for RDA on the thermocline samples, biomarkers that were  
297 identified in fewer than three samples were designated “rare species” and were excluded from the analysis  
298 (GDGT-DH-0, GDGT-DH-1 and OH-GDGT-HPH-0 excluded). This is because outliers can violate the  
299 linearity of the relationship between the response and explanatory variables (Legendre & Legendre, 2012).  
300 Samples CTD 1 and 25 were also excluded from the analysis. CTD 1 is located offshore of the Falkland  
301 Islands and is the only sample from North of the SAF, thus representing the only data point for the  
302 Subantarctic Zone of the Southern Ocean that is unlikely to be representative for the polar environment. CTD  
303 25, located close to South Georgia, was excluded due to high biomarker abundances (Figure 4a) which could  
304 be due to exceptionally high productivity in this area (e.g. Atkinson et al., 2001). Variance inflation factors  
305 (VIFs) for the response variables were between 3.5 (fluorescence) and 11.4 (oxygen concentration)  
306 (Supplement C Table 1). The VIF for oxygen concentration is slightly higher than is typically acceptable for  
307 RDA analysis. This is due to correlation between oxygen concentration and fluorescence ( $R_2=0.63$ ),  
308 however, as the  $R_2$  is below 0.7 this is unlikely to violate the assumptions of the RDA (Legendre &  
309 Legendre, 2012) (Supplement C Table 2). RDA shows 64% constrained variation with RDA1 and 2

310 accounting for 63% of the cumulative variation (Supplement C Tables 3-5). The RDA is statistically  
311 significant ( $p < 0.05$ ,  $f = 3.5$ ), furthermore, RDA1 is found to be statistically significant ( $p < 0.05$ ,  $f = 11.48$ )  
312 however, RDA2 is not significant ( $p = 0.42$ ,  $f = 2.35$ ) (Supplement C Tables 10-12). Species scores show HPH-  
313 GDGT-0 and HPH-cren to load positive on RDA 1, with MH-GDGT-0, MH-cren, MH-OH-GDGT-MH-0,  
314 DH-OH-GDGT-0, and MH-MH-diOH-GDGT-0 loading highly negative on RDA1 (Figure 5). Of the  
315 explanatory variables tested, temperature is statistically significant at the  $< 0.05$  level ( $f = 8.56$ ) and with  
316 salinity ( $p = 0.07$ ,  $f = 2.61$ ) and oxygen concentration ( $p = 0.09$ ,  $f = 2.58$ ) approaching significance (Supplement  
317 C Table 12). The site scores show CTD 20, 21, 22, 23, and 24 to be negatively loaded on RDA1 with CTD 3,  
318 5, 7, 10, 13, 16, 18 and 19 to be positively loaded on RDA1 suggesting that these stations are contrasted  
319 along this axis (Figure 5).

## 320 **4. Discussion**

### 321 **4.1. Hydroxylated GDGTs in Polar Environments**

322 In this study, two hydroxylated GDGTs (OH-GDGT-0 and diOH-GDGT-0) were detected. Hydroxylated  
323 GDGTs have been reported as potential biomarkers for reconstructing ocean temperature change in cold  
324 waters (Fietz et al., 2013, 2016) and in this study contribute up to 49.8% (OH-GDGT) and 30.1% (diOH-  
325 GDGT) of total IPL-GDGTs. Hydroxylated IPL-GDGTs are not commonly reported in previous SPM  
326 studies (e.g. Kim et al., 2016; Kang et al., 2017; Hurley et al., 2018). However, these compounds have been  
327 reported as c-GDGTs in marine and lacustrine sediments, with hydroxylated GDGTs found to contribute  
328 approximately 8% in marine sediments from temperate and tropical sites (Liu et al., 2012; Lu et al., 2015).  
329 These compounds have been reported in much higher abundance in polar environments including up to 20%  
330 in SPM and up to 16% in surface sediments from the Nordic Seas (Fietz et al., 2013) and up to 20% in  
331 surface sediments from the Southern Ocean (Huguet et al., 2013).  
332 Exceptionally high hydroxylated GDGT relative abundances of greater than 20% could be due to differences  
333 in methodologies to the previous studies which measured core GDGTs by atmospheric pressure chemical  
334 ionisation (APCI; Liu et al., 2012; Fietz et al., 2013; Huguet et al., 2013; Lu et al., 2015) while this study  
335 examined IPL-GDGTs using electrospray ionisation (ESI). Using the same LC-MS methodology, Sollai et  
336 al. (2019a) report average hydroxylated IPL-GDGT relative abundances of 22% ( $\pm 19\%$ ) with a range of 0-  
337 51% in SPM from the euxinic Black Sea; however, similar analyses from the Arabian Sea (Besseling et al.,

338 2018), the eastern tropical South Pacific (Sollai et al., 2019b) and the Mediterranean Sea did not detect  
339 hydroxylated IPL-GDGTs. Molecular dynamics simulations have shown that the addition of hydroxyl  
340 moieties in the tetraether structure increases the fluidity of the cell membrane and aid trans-membrane  
341 transport in cold environments (Huguet et al., 2017). The exceptionally high amount of hydroxylated IPL-  
342 GDGT for the Amundsen and Scotia seas may therefore be due to elevated synthesis of these biomarkers in  
343 cold environments.

#### 344 **4.2. IPL-GDGT Distributions as an Indicator of Archaeal Populations**

345 In both the Amundsen and Scotia Sea samples low diversity of cyclic GDGTs is observed (RI ranging from  
346 0.02 – 1 for the Scotia Sea and 0.03 – 0.9 for the Amundsen Sea; Tables 1 and 2). This is particularly low  
347 compared with the RI of the global core top calibration, which includes a range of Southern Ocean samples,  
348 reporting an RI range of 1.25-3 (excluding the Red Sea samples; Kim et al., 2010; Ho et al., 2011, 2014;  
349 Zhang et al., 2016). Previous SPM studies spanning a range of marine habitats have reported the presence of  
350 hydroxylated GDGT-1, -2, and -3 as well as a wider range of non-hydroxylated GDGTs, such as GDGT-3  
351 and -4 (Kim et al., 2016; Besseling et al., 2018; Hurley et al., 2018; Sollai et al., 2019a,b). As this study used  
352 the same analytical methodology as Besseling et al. (2018) and Sollai et al. (2019a,b), these differences  
353 cannot be attributed to analytical methodologies. Low cyclic diversity of GDGTs in the Amundsen and  
354 Scotia seas could be due to differences in the synthesis of these lipids by the source Thaumarchaeota. The  
355 relationship between ocean temperature and the cyclicity of GDGTs has been firmly established, with  
356 increasing ocean temperatures correlated with increasing relative abundance of GDGTs with 2 or more  
357 cyclopentane moieties (Schouten et al., 2002, 2007; Kim et al., 2008, 2010). However, Kim et al. (2010) note  
358 some differences between sub-tropical and sub-polar oceans, with cren playing a more important role in  
359 temperature reconstructions in the subtropics than in polar oceans, suggesting that there may be differences  
360 in membrane adaptation strategies of Thaumarchaeota. Principal component analysis of IPL-GDGT  
361 distributions of a moderately thermophilic Thaumarchaeota along with previously published data identifies  
362 two distinct clusters with a clear partition between the orders of Nitrosopumilales and Nitrososphaeales (Bale  
363 et al., 2019). IPL-GDGTs analysed in this study cluster within the Nitrosopumilales group due to the high  
364 relative abundances of GDGT-0 and low relative abundances of all other GDGTs. Due to the polar locations  
365 of the Amundsen and Scotia Sea samples, Nitrosopumilales are likely to be the key AOA in these

366 environments. Previous microbial analysis of the spatial variation in prokaryotes of the Amundsen Sea  
367 polynya identified the most abundant Thaumarchaea marine group I (MGI) sequence belonged to the cluster  
368 affiliated with “*Ca. Nitrosopumilus maritimus*” (Kim et al., 2014). In similar studies within the wider  
369 Southern Ocean region phylogenetic analysis reveals high abundances of sequences clustering with  
370 *Nitrosopumilus*. Hernandez et al. (2015) analysed surface water samples from Potter Cove (King George  
371 Island, wester Antarctica Peninsula) which revealed that the majority of sequences fell into the clade  
372 containing “*Ca. Nitrosopumilus maritimus*” and other environmental sequences containing Thaumarchaeota.  
373 Signori et al. (2018) studied microbial spatial and temporal variability at 10 stations off the Antarctic  
374 peninsula revealing spring to be characterised by SAR11 and microbial communities remaining from winter,  
375 including Thaumarchaeota (*Nitrosopumilus*), Euryarchaeota, and SAR324, with a shift in microbial  
376 populations during the summer and autumn.

377 Three polar head groups were detected in this study, i.e. MH, DH, and HPH. All three head groups have  
378 previously been identified in culture (Schouten et al., 2008; Pitcher et al., 2011; Sinninghe Damsté et al.,  
379 2012; Elling et al., 2017), environmental studies (e.g. Zhu et al., 2016; Besseling et al., 2018), and have  
380 widely been associated with Thaumarchaeota. It has been postulated that specific IPL-GDGTs may be  
381 associated with particular Thaumarchaeotal groups or habitats (Sinninghe Damsté et al., 2012; Elling et al.,  
382 2017; Bale et al., 2019). Previously the HPH head group has been associated with the Nitrosopumilales order  
383 (Group I.1a) and the DH head group with the Nitrosophaeales order (Group I.1b) (Sinninghe Damsté et al.,  
384 2012). More recent studies have shown that environmental niche or habitat may be the main driver of GDGT  
385 head group composition rather than phylogeny (Elling et al., 2017; Bale et al., 2019). Relevant to this study,  
386 Elling et al. (2017) analysed the lipidome of 10 Thaumarchaeotal cultures and identified DH-GDGTs and DH-  
387 OH-GDGTs as key membrane components of the marine mesophiles compared with the terrestrial  
388 thermophilic and soil mesophilic Thaumarchaeota. In the present study, high abundances of HPH were  
389 detected, contributing up to 92.9% and up to 100% of total IPL-GDGTs in the Amundsen Sea and Scotia Sea  
390 respectively. The dominance of HPH in the lipid profiles of the Amundsen and Scotia seas align with  
391 previous culture analysis (Schouten et al., 2008; Pitcher et al., 2011; Sinninghe Damsté et al., 2012; Elling et  
392 al., 2017).

### 393 **4.3. Distribution of IPL-GDGTs in surface waters of Southern Ocean**

394 In this study, we observed a number of consistent trends in the water column IPL-GDGT distributions  
395 between the different Amundsen Sea and Scotia Sea sampling stations. In the surface samples, collected  
396 within the euphotic zone of the Amundsen Sea at PS104/017 (10 m), PS104/022 (10 m and 30 m),  
397 PS104/043 (10 m), and the Scotia sea (15-40m depth at CTD stations 3, 5, 7, 10, 13, 18, 19, 22, 23, 24, 25)  
398 no IPL-GDGTs were identified. Previous studies from the Southern Ocean have shown water column  
399 archaeal distributions to be highly variable on both a temporal and spatial scale. Broadly, archaea (as  
400 measured by cell counts or rRNA) are often absent or found in relatively low abundance in the surface  
401 waters during the austral spring algal bloom and during austral summer (Massana et al., 1998; Church et al.,  
402 2003; Kalanetra et al., 2009; Besseling et al., 2020). The absence of archaea in the surface waters of the  
403 Southern Ocean contrasts with the high abundance of bacteria and is part of a larger seasonal cycle in  
404 archaeal population dynamics (Church et al., 2003). Temporal distributions of archaea are then shown to  
405 become more evenly distributed by depth, with an increase in the population within the surface waters  
406 throughout austral autumn-winter (Church et al., 2003). The Amundsen Sea samples were collected during  
407 austral summer. Two previous studies in the Antarctic Peninsula have shown an increase in group I archaeal  
408 populations in surface waters during austral summer and winter (Massana et al., 1998; Murray et al., 1998).  
409 However, Kalanetra et al. (2009) did not observe any archaea in surface waters west of the Antarctic  
410 Peninsula during austral summer. The mechanism for this temporal heterogeneity is likely mediated by a  
411 combination of physical and biological factors including, water mass properties, concentrations of dissolved  
412 and particulate organic carbon (Murray et al., 1998). Furthermore, the absence of AOA in the surface waters  
413 during austral spring, when primary productivity is highest, could be due to competition with bacteria and  
414 algae that bloom during the same time period and/or a subsequent nutrient limitation (Massana et al., 1998;  
415 Church et al., 2003; Kalanetra et al., 2009). As the current study was only performed at one time point during  
416 austral summer a larger sampling campaign would be required to fully characterise microbial and IPL-  
417 GDGT seasonality in the Amundsen Sea.

418 In contrast with the other stations, the surface water samples from PS104/003 and PS104/007 (10 m and 20  
419 m respectively) and CTD 1, 16, 20, and 21 were found to contain IPLs. The samples from PS104/007 (10 m),  
420 CTD 20 and 21 only contained the MH head group. It should be noted that while the MH head group is

421 known to be synthesised by archaea (e.g. Sinninghe Damsté et al., 2012), this IPL is recalcitrant and can be  
422 formed as a degradation product of other IPL-GDGTs (e.g. Lengger et al., 2013, 2014). In contrast, HPH is  
423 more labile and less readily preserved in sediments following cell death and is hence considered to be a  
424 biomarker for recently active archaea and, in particular, Thaumarchaeota (Pitcher et al., 2010; Sinninghe  
425 Damsté et al., 2012). HPH-cren can vary between phylogenetic subgroups (Elling et al., 2017) and while DH  
426 head group is not as labile as HPH due to its glycosidic structure (Lengger et al., 2013), DH-GDGTs have  
427 been identified with consistent relative abundances across the Nitrosopumilales order (Group 1.1a),  
428 suggesting DH-cren as an additional biomarker for AOA activity (Elling et al., 2017). Hence, the dominance  
429 of the MH head group at these stations may indicate an inactive/relic archaeal population at this depth.  
430 Higher IPL-GDGT diversity was detected at PS104/003 and CTD 1 and 16 including HPH and DH head  
431 groups indicating a recently active archaeal population (Sinninghe Damsté et al., 2012; Elling et al., 2017).  
432 PS104/003 is located in an area of active upwelling of nutrient-rich waters largely composed of CDW (Pine  
433 Island Bay polynya) (Mankoff et al., 2012). Together with the Amundsen Polynya located north of Dotson  
434 and westernmost Getz ice shelves (Figure 1), it is one of the most productive regions (per unit area) of the  
435 Southern Ocean (Arrigo and van Dijken, 2003). Productivity is further aided by the influx of iron released  
436 from the rapidly melting Thwaites and Pine Island glaciers (Alderkamp et al., 2012; Gerringa et al., 2012;  
437 Thuroczy et al., 2012; St-Laurent et al., 2017). Results from another cruise in the region identified that  
438 productivity is limited not only by nutrient and iron availability but also by light; productivity is 30-50%  
439 lower in the Pine Island Polynya compared to the Amundsen Polynya, with this difference attributed to the  
440 significant difference in solar irradiance levels between the two polynyas throughout the summer season  
441 (Park et al., 2017). Similarly, CTD 1 is located close to the Falkland Islands in the Subantarctic Zone north  
442 of the SAF and is potentially subject to additional terrestrial inputs and coastal dynamics. Kalanetra et al.  
443 (2009) suggests that a combination of both light and nutrient differences between Arctic and Antarctic ocean  
444 settings could cause the differences in archaeal populations in the surface ocean, where low light and nutrient  
445 levels in the surface allows archaeal populations to flourish, with further studies suggesting photoinhibition  
446 of Thaumarchaeota (Church et al., 2003; Mincer et al., 2007; Hu et al., 2011; Merbt et al., 2012; Luo et al.,  
447 2014).



#### 448 **4.4. Influence of Circumpolar Deep Water on IPL Distributions: Amundsen Sea**

449 IPL-GDGT diversity increased downwards in the water column through the thermocline and the CDW layer  
450 in the Amundsen Sea (Table 3). DH-cren and HPH-cren may be widely applied as biomarkers for recently  
451 active Thaumarchaeota populations having been identified as key cell membrane lipids (Pitcher et al., 2010;  
452 Sinninghe Damsté et al., 2012; Elling et al., 2017). HPH-cren was identified consistently throughout the  
453 thermocline and CDW layer at all Amundsen Sea stations (Table 3). Our results, therefore, suggest recently  
454 active AOA at the thermocline and within the CDW. Tolar et al. (2016) shows ammonia oxidation (AO) to  
455 occur throughout the water column, with similar rates of AO in CDW during both winter and summer  
456 seasons and increased AO in surface waters during the late winter in sites west of the Antarctic Peninsula.  
457 These patterns in AO are consistent with molecular microbiology studies from the Amundsen Sea and  
458 Antarctic Peninsula region that identified Thaumarchaeota throughout the water column, but with a seasonal  
459 trend where these archaea are often absent in the surface waters during spring and summer, and present in the  
460 CDW throughout the year (Massana et al., 1998; Alonso-Saez et al., 2011). HPH-cren, however, may not be  
461 the most suitable proxy for tracking the complete AOA population as the relative abundance of this IPL can  
462 vary significantly between phylogenetic subgroups (Elling et al., 2017). DH-GDGTs have been identified  
463 with consistent relative abundances across the Nitrosopumilales order (Group 1.1a), suggesting DH-cren as  
464 an additional biomarker for AOA activity (Elling et al., 2017). In this study we detect DH-cren consistently  
465 in the CDW layer and with low relative abundance in the thermocline of PS104/003 and PS104/007 and  
466 absence in the thermocline waters at PS104/017 and PS104/022. Thaumarchaeota are thought to partition  
467 between shallow water (0-130 m) and deep water (500-4000 m) marine clades (Francis et al., 2005; Hallam  
468 et al., 2006). Therefore, the depth trend of HPH-cren throughout the thermocline and CDW and DH-cren  
469 restricted to CDW depths could reflect differences in Thaumarchaeota populations in the Amundsen Sea.  
470 While the data presented here provide only a snapshot of the Amundsen Sea IPL-GDGT distributions, this  
471 small contrast in HPH and DH-cren distributions may represent a significant partition between  
472 Thaumarchaeota populations and warrants further analysis. Thaumarchaeota are not homogeneously  
473 distributed throughout the water column. Molecular microbiology has identified Thaumarchaeota to be  
474 virtually absent from Antarctic Summer Surface Waters (0-45m depth) and present in Winter Water (45-  
475 105m depth) and Circumpolar Deep Water (105-3500m depth) (e.g. Kalanetra et al., 2009). Our observation

476 of active IPL-GDGT synthesis within the CDW has implications for the use of c-GDGT based biomarker  
477 proxies in the Amundsen Sea and potentially more broadly within the Southern Ocean. Indeed, temperature  
478 reconstructions based on GDGTs are suggested to represent the 45-200m range (Kim et al., 2012),  
479 acknowledging the absence of Thaumarchaeota from the surface waters during the summer months in  
480 Antarctica. The influence of CDW on reconstructed TEX<sub>86</sub> paleo temperatures has been hypothesised in  
481 Adélie Land (East Antarctica) with Kim et al. (2012) suggesting warmer reconstructed temperatures were  
482 likely due to the upwelling of CDW onto the piston core site. In our study we specifically observe IPL-  
483 GDGTs of recently living archaea in the CDW (over 500 m water depth). Furthermore, we observe a shift in  
484 head group composition at CDW depths in the Amundsen sea representing a shift in the IPL-GDGT  
485 producing community. We hypothesise that the contribution of GDGTs synthesised at CDW depths where  
486 physical parameters (e.g. temperature) can be strikingly different to the 45-200m water depth may have a  
487 significant impact on reconstructed TEX<sub>86</sub> temperatures, not only the Amundsen Sea but potentially more  
488 broadly within the Southern Ocean.

#### 489 **4.5. Influences on the GDGT-IPL distribution along the Scotia Sea Transect**

490 IPL-GDGTs were found to be present within the thermocline (60-110 m) and contain a high proportion of  
491 MH head group IPL-GDGTs, suggesting a high proportion of relic IPL-GDGTs in the Scotia Sea that could  
492 relate to the seasonality of archaeal populations. Further to this, DH-cren was found to be absent from the  
493 thermocline with HPH-cren intermittently present. This pattern in DH-cren and HPH-cren in the Scotia Sea  
494 is consistent with our results from the Amundsen Sea where DH-cren was mostly absent from the 120-240m  
495 depth intervals but present in the CDW depth intervals (i.e. below 400m), while HPH-cren was present at  
496 both the thermocline and CDW depths.

497 The Scotia Sea samples were collected along clear temperature (-1.6 to +7.3 °C), salinity (33.6 -34.3 PSU),  
498 oxygen (218.3-332.7 µmol/kg), and fluorescence (0.03-1.1 ml/m<sup>3</sup>) gradients associated with ocean fronts,  
499 which are known to impact bacterioplankton population diversity (Wilkins et al., 2013; Baltar et al., 2016;  
500 Raes et al., 2018). Figure 5 shows that higher latitude samples with cooler ocean temperatures cluster  
501 positively on RDA axis 1 and have higher relative abundances of HPH-GDGT-0 and HPH-cren (samples 3,  
502 5, 7, 10, 13, 16, 18, 19), whilst samples from warmer ocean waters and lower latitudes cluster negatively on  
503 RDA axis 1 and have higher relative abundances of MH and DH IPL-GDGTs (samples 20 – 24). The

504 contrast in IPL headgroup distributions between CTD stations 3-19 and 20-24 suggests that RDA 1  
505 represents the transition across the SBACC. Temperature was found to be statistically significant explanatory  
506 variable in the RDA which is consistent with previous research that has identified clear links between core  
507 GDGT relative abundances and environmental variables such as temperature (Schouten et al., 2007; Kim et  
508 al., 2008, 2010). Specifically, we observe a shift in the GDGT head group between the warmer and cooler  
509 waters of the ACC fronts. Temperature, along with other physicochemical properties (e.g. nutrient and  
510 oxygen concentrations) vary across the ACC (e.g. Rubin, 2003; Freeman et al., 2019). These shifts in  
511 physicochemical properties across permanent oceanic boundaries influence and control bacterial and  
512 archaeal species richness, creating ecological boundaries or niches (e.g. Raes et al., 2018). Variability in IPL-  
513 GDGT headgroup composition observed across the Scotia Sea transect could reflect the transition across an  
514 environmental niche (e.g. Elling et al., 2017; Bale et al., 2019). As this study is limited by the number of  
515 chemical properties analysed, it would be speculative to infer the relative importance of specific nutrient  
516 concentrations across the Scotia Sea transect.

517 Alternatively, the shift in IPL-GDGT head group could also be influenced by the presence of the Weddell  
518 Gyre which is located south of 55-60 °S, and between 60 °W and 30 °E (Vernet et al., 2019). The Weddell  
519 Gyre is a region of enhanced productivity, with austral summer chlorophyll *a* concentrations ranging from  
520 1.5-10 mg m<sup>-3</sup> (Bathmann et al., 1997; Cape et al. 2014) due to high concentrations of nutrients upwelled and  
521 circulated through the gyre (Vernet et al., 2019 and references therein).

## 522 **5. Conclusions**

523 A range of archaeal IPLs was detected in both the Amundsen Sea and the Scotia Sea. High relative  
524 abundances of OH-GDGT core type were observed which could reflect the polar environmental setting of  
525 these samples. Low cyclicity was detected in both the Amundsen and Scotia Seas for both the GDGT and  
526 OH-GDGT core type with acyclic OH-GDGT-0 and GDGT-0, -1, -2, and cren reported. Low cyclicity of  
527 GDGTs may potentially be a more widespread feature of the Southern Ocean GDGT signature.  
528 IPL-GDGT relative abundance along the Scotia Sea transect shows a distinct pattern across the  
529 oceanographic front transition. Samples south of the SBACC and from cooler ocean waters had higher  
530 relative abundances of HPH-GDGT-0 and HPH-cren compared with samples north of the SBACC, and while  
531 those from warmer ocean waters had higher relative abundances of MH and DH IPL-GDGTs. Indeed, RDA

532 reveals that temperature is a significant explanatory variable, however, productivity and nutrient availability  
533 may also play a role in IPL-GDGT distributions. Additionally, this shift in IPL-GDGT distributions could  
534 represent a shift in the dominant archaeal IPL synthesisers and/or a physiological survival strategy.

535 In the Amundsen Sea IPL-GDGTs are detected throughout the water column. IPL-GDGTs of recently living  
536 archaea were specifically observed in the CDW (over 500 m water depth) along with a shift in head group  
537 composition at CDW depths representing a shift in the IPL-GDGT producing community. We hypothesise  
538 that the contribution of GDGTs synthesised at CDW depths where physical parameters, such as temperature,  
539 can be strikingly different to the upper water column (e.g. 0-200m water depth) may have a significant  
540 impact on reconstructed TEX<sub>86</sub><sup>L</sup> temperatures in not only the Amundsen sea but potentially more broadly  
541 within the Southern Ocean.

542

#### 543 Data availability

544 CTD data from JR257/JR272A are available from the British Oceanographic Data Centre at  
545 <https://www.bodc.ac.uk/data/documents/cruise/11431/>.

#### 546 Author contributions

547 CSJ, ELM, CDH, EM, JAS designed the experiments. CSJ, NJB, ECH, JM undertook the laboratory  
548 preparation and analysis. EPA, CA, TB, VP generated the oceanographic data. CSJ and AS undertook  
549 statistical analysis. CSJ, ELM, NJB, ECH, SS, JAS wrote the manuscript with contributions from all authors.

#### 550 Competing interests

551 The authors declare that they have no conflicting interests.

#### 552 Acknowledgments

553 This project was funded through a UK Natural Environment Research Council (NERC) Standard Grant,  
554 awarded to JS, ELM, CDH, and Kate Hendry (NE/M013081/1), a British Antarctic Survey Collaborative  
555 Gearing Scheme award (ELM), a Helmholtz Research Grant (VH-NG-1101; JM), and the Durham  
556 University Department of Geography Research Development Fund (CSJ). N.B. is funded by the European  
557 Research Council (ERC) under the European Union's Horizon 2020 research and innovation program (grant  
558 agreement no.694569). Collection of CTD casts on the A23 transect was supported by NERC National  
559 Capability funding to BAS. We thank M.D. West, A.J. Hayton, and D. Dorhout for technical support. We  
560 are grateful to the captains, crews, support staff and scientists participating in cruises JR257, JR272 and

561 PS104, and acknowledge funding for cruise PS104 by AWI, MARUM, BAS and NERC UK-IODP. Lastly,  
562 we thank two anonymous reviewers for their constructive comments that improved the manuscript.

## 563 **6. References**

564 Alderkamp, A.-C., Mills, M. M., van Dijken, G. L., Laan, P., Thuroczy, C.-E., Gerringa, L. J. A., de Baar, H.  
565 J. W., Payne, C. D., Visser, R. J. W., Buma, A. G. J. and Arrigo, K. R.: Iron from melting glaciers fuels  
566 phytoplankton blooms in the Amundsen Sea (Southern Ocean): Phytoplankton characteristics and  
567 productivity, *Deep-Sea Res. Part II- Top. Stud. Oceanogr.*, 71–76, 32–48,  
568 <https://doi.org/10.1016/j.dsr2.2012.03.005>, 2012.

569 Allen, C. S., Peck, V. L., Graham, A. G. C., Blagbrough, H., Robinson, M. W. and McClymont, E.: RRS  
570 James Clark Ross Marine Science Cruises JR257 and JR254e, March-April 2012, British Antarctic Survey,  
571 Cambridge, UK, [https://www.bodc.ac.uk/resources/inventories/cruise\\_inventory/reports/jr257\\_254e.pdf](https://www.bodc.ac.uk/resources/inventories/cruise_inventory/reports/jr257_254e.pdf),  
572 2012.

573 Alonso-Saez, L., Sanchez, O., Gasol, J. M., Balague, V. and Pedros-Alio, C.: Winter-to-summer changes in  
574 the composition and single-cell activity of near-surface Arctic prokaryotes, *Environ. Microbiol.*, 10, 2444–  
575 2454, <https://doi.org/10.1111/j.1462-2920.2008.01674.x>, 2008.

576 Alonso-Saez, L., Andersson, A., Heinrich, F. and Bertilsson, S.: High archaeal diversity in Antarctic  
577 circumpolar deep waters, *Environ. Microbiol. Rep.*, 3, 689–697, <https://doi.org/10.1111/j.1758-2229.2011.00282.x>, 2011.

579 Arrigo, K. and van Dijken, G.: Phytoplankton dynamics within 37 Antarctic coastal polynya systems, *J.*  
580 *Geophys. Res. – Oceans.*, 108, <https://doi.org/10.1029/2002JC001739>, 2003.

581 Atkinson, A., Whitehouse, M.J., Priddle, J., Cripps, G.C., Ward, P. and Brandon, M.A.: South Georgia,  
582 Antarctic: a productive, cold water, pelagic ecosystem, *Mar.Ecol.Prog.Ser.*, 216, 279-308,  
583 <https://doi.org/10.3354/meps216279>, 2001.

584 Bale, N.J., Palatinszky, M., Rijpstra, W.I.C., Herbold, C.W., Wagner, M., Sinninghe Damsté, J.S.:  
585 Membrane lipid composition of the moderately thermophilic ammonia-oxidising archaeon “*Candidatus*  
586 *Nitrosotenuis uzonensis*” at different growth temperatures. *Appl. Environ. Microbiol.*, 85, <https://doi.org/10.1128/AEM.01332-19>, 2019.

588 Baltar, F., Currie, K., Stuck, E., Roosa, S. and Morales, S. E.: Oceanic fronts: transition zones for  
589 bacterioplankton community composition, *Environ. Microbiol. Rep.*, 8, 132–138,  
590 <https://doi.org/10.1111/1758-2229.12362>, 2016.

591 Bathmann, U.V., Scharek, R., Klaas, C., Dubischar, C.D. and Smetacek, V.: Spring development of  
592 phytoplankton biomass and composition in major water masses of the Atlantic sector of the Southern Ocean,  
593 *Deep Sea Res. Part II Top. Stud. Oceanogr.* 44, 51-67, [https://doi.org/10.1016/S0967-0645\(96\)00063-X](https://doi.org/10.1016/S0967-0645(96)00063-X),  
594 1997.

595 Bauersachs, T., Speelman, E. N., Hopmans, E. C., Reichart, G. J., Schouten, S. and Sinninghe Damsté, J. S.:  
596 Fossilized glycolipids reveal past oceanic N<sub>2</sub> fixation by heterocystous cyanobacteria, *Proc. Natl. Acad. Sci.*  
597 *U. S. A.*, 107, 19190–19194, <https://doi.org/10.1073/pnas.1007526107>, 2010.

598 Besseling, M. A., Hopmans, E. C., Boschman, R. C., Sinninghe Damsté, J. S. and Villanueva, L.: Benthic  
599 archaea as potential sources of tetraether membrane lipids in sediments across an oxygen minimum zone,  
600 *Biogeosciences*, 15, 4047–4064, <https://doi.org/10.5194/bg-15-4047-2018>, 2018.

601 Besseling, M. A., Hopmans, E. C., Bale, N. J., Schouten, S., Sinninghe Damsté, J. S. and Villanueva, L.: The  
602 absence of intact polar lipid-derived GDGTs in marine waters dominated by Marine Group II: Implications  
603 for lipid biosynthesis in Archaea. *Sci. Rep.*, 10, <https://doi.org/10.1038/s41598-019-57035-0>, 2020.

604 Brochier-Armanet, C., Boussau, B., Gribaldo, S. and Forterre, P.: Mesophilic crenarchaeota: proposal for a  
605 third archaeal phylum, the Thaumarchaeota, *Nat. Rev. Microbiol.*, 6, 245–252,  
606 <https://doi.org/10.1038/nrmicro1852>, 2008.

607 Cape, M.R., Vernet, M., Kahru, M. and Spreen, G.: Polynya dynamics drive primary production in the  
608 Larsen A and B embayments following ice shelf collapse, *J. Geophys. Res. Oceans*, 119, 572-594,  
609 <https://doi.org/10.1002/2013JC009441>, 2014.

610 Carter, L., McCave, I. N. and Williams, M. J. M.: Circulation and water masses of the Southern Ocean: A  
611 Review, *Antarct. Clim. Evol.*, 8, 85–114, [https://doi.org/10.1016/S1571-9197\(08\)00004-9](https://doi.org/10.1016/S1571-9197(08)00004-9), 2009.

612 Church, M. J., DeLong, E. F., Ducklow, H. W., Karner, M. B., Preston, C. M. and Karl, D. M.: Abundance  
613 and distribution of planktonic Archaea and Bacteria in the waters west of the Antarctic Peninsula, *Limnol.*  
614 *Oceanogr.*, 48, 1893–1902, <https://doi.org/10.4319/lo.2003.48.5.1893>, 2003.

615 Darfeuil, S., Menot, G., Giraud, X., Rostek, F., Tachikaea, K., Garcia, M. and Bard, E.: Sea surface  
616 temperature reconstructions over the last 70 kyr off Portugal: Biomarker data and regional modelling,  
617 *Paleoceanogr. Paleoclimatol.* 31, 40-65, [https://doi.org/ 10.1002/2015PA002831](https://doi.org/10.1002/2015PA002831), 2016.

618 Delong, E. F., Wu, K. Y., Prezelin, B. B. and Jovine, R. V. M.: High abundance of archaea in Antarctic  
619 marine picoplankton, *Nature*, 371, 695–697, <https://doi.org/10.1038/371695a0>, 1994.

620 Elling, F. J., Konneke, M., Lipp, J. S., Becker, K. W., Gagen, E. J. and Hinrichs, K. U.: Effects of growth  
621 phase on the membrane lipid composition of the thaumarchaeon *Nitrosopumilus maritimus* and their  
622 implications for archaeal lipid distributions in the marine environment, *Geochim. Cosmochim. Acta*, 141,  
623 579–597, <https://doi.org/10.1016/j.gca.2014.07.005>, 2014.

624 Elling, F. J., Konneke, M., Nicol, G. W., Stieglmeier, M., Bayer, B., Spieck, E., de la Torre, J. R., Becker, K.  
625 W., Thomm, M., Prosser, J. I., Herndl, G. J., Schleper, C. and Hinrichs, K. U.: Chemotaxonomic  
626 characterisation of the Thaumarchaeal lipidome, *Environ. Microbiol.*, 19, 2681–2700,  
627 <https://doi.org/10.1111/1462-2920.13759>, 2017.

628 Etourneau, J., Collins, L. G., Willmott, V., Kim, J. H., Barbara, L., Leventer, A., Schouten, S., Sinninghe  
629 Damsté, J. S., Bianchini, A., Klein, V., Crosta, X. and Massé, G.: Holocene climate variations in the western  
630 Antarctic Peninsula: evidence for sea ice extent predominantly controlled by changes in insolation and  
631 ENSO variability, *Clim. Past*, 9, 1431–1446, <https://doi.org/10.5194/cp-9-1431-2013>, 2013.

632 Etourneau, J., Sgubin, G., Crosta, X., Swingedouw, D., Willmott, V., Barbara, L., Houssais, M-N., Schouten,  
633 S., Sinninghe Damsté, J.S., Goosse, H., Escutia, C., Crespin, J., Massé, G. and Kim, J-H.: Ocean temperature  
634 impact on ice shelf extent in the eastern Antarctic Peninsula, *Nat. Commun.* 10, 1-8,  
635 <https://doi.org/10.1038/s41467-018-08195-6>, 2019.

636 Evans, T. W., Wormer, L., Lever, M. A., Lipp, J. S., Lagostina, L., Lin, Y. S., Jorgensen, B. B. and Hinrichs,  
637 K. U.: Size and composition of seafloor microbial community in the Benguela upwelling area examined  
638 from intact membrane lipid and DNA analysis, *Org. Geochem.*, 111, 86–100,  
639 <https://doi.org/10.1016/j.orggeochem.2017.06.008>, 2017.

640 Fietz, S., Huguet, C., Rueda, G., Hambach, B. and Rosell-Melé, A.: Hydroxylated isoprenoidal GDGTs in  
641 the Nordic Seas, *Mar. Chem.*, 152, 1–10, <https://doi.org/10.1016/j.marchem.2013.02.007>, 2013.

642 Fietz, S., Ho, S. L., Huguet, C., Rosell-Mele, A. and Martinez-Garcia, A.: Appraising GDGT-based seawater  
643 temperature indices in the Southern Ocean, *Org. Geochem.*, 102, 93–105,  
644 <https://doi.org/10.1016/j.orggeochem.2016.10.003>, 2016.

645 Francis, C. A., Roberts, K. J., Beman, J. M., Santoro, A. E. and Oakley, B. B.: Ubiquity and diversity of  
646 ammonia-oxidizing archaea in water columns and sediments of the ocean, *Proc. Natl. Acad. Sci. U. S. A.*,  
647 102, 14683–14688, <https://doi.org/10.1073/pnas.0506625102>, 2005.

648 Freeman, N. M., Munro, D. R., Sprintall, J., Mazloff, M. R., Purkey, S., Rosso, I., DeRanek, C. A. and  
649 Sweeney, C.: The observed seasonal cycle of macronutrients in Drake Passage: Relationship to fronts and  
650 utility as a model metric, *J. Geophys. Res. Oceans*, 124, 4763–4783, <https://doi.org/10.1029/2019JC015052>,  
651 2019.

652 Gerringa, L. J. A., Alderkamp, A.-C., Laan, P., Thuroczy, C.-E., De Baar, H. J. W., Mills, M. M., van  
653 Dijken, G. L., van Haren, H. and Arrigo, K. R.: Iron from melting glaciers fuels the phytoplankton blooms in  
654 Amundsen Sea (Southern Ocean): Iron biogeochemistry, *Deep-Sea Res. Part II- Top. Stud. Oceanogr.*, 71–  
655 76, 16–31, <https://doi.org/10.1016/j.dsr2.2012.03.007>, 2012.

656 Gohl, K.: The Expedition PS104 of the Research Vessel POLARSTERN to the Amundsen Sea in 2017,  
657 Alfred-Wegener-Institut, Helmholtz-Zentrum für Polar- und Meeresforschung;, Bremerhaven, Germany,  
658 [https://doi.org/10.2312/BzPM\\_0712\\_2017](https://doi.org/10.2312/BzPM_0712_2017), 2017.

659 Hallam, S. J., Mincer, T. J., Schleper, C., Preston, C. M., Roberts, K., Richardson, P. M. and DeLong, E. F.:  
660 Pathways of carbon assimilation and ammonia oxidation suggested by environmental genomic analyses of  
661 marine Crenarchaeota, *Plos Biol.*, 4, 520–536, <https://doi.org/10.1371/journal.pbio.0040095>, 2006.

662 Hernandez, E.A., Piquet, A.M.T., Lopez, J.L., Buma, A.G.J. and Mac Cormack, W.P.: Marine archaeal  
663 community structure from Potter Cove, Antarctica: high temporal and spatial dominance of the phylum  
664 Thaumarchaeota, *Polar. Biol.*, 38, 117-130, <https://doi.org/10.1007/s00300-014-1569-8>, 2015

665 Heywood, K. J., Naveira Garabato, A. C. and Stevens, D. P.: High mixing rates in the abyssal Southern  
666 Ocean, *Nature*, 415, 1011–1014, <https://doi.org/10.1038/4151011a>, 2002.

667 Hillenbrand, C.-D., Smith, J.A., Hodell, D.A., Greaves, M., Poole, C.R., Kender, S., Williams, M.,  
668 Andersen, T.J., Jernas, P.E., Elderfield, H., Klages, J.P., Roberts, S.J., Gohl, K., Larter, R.D. and Kuhn, G.:



669 West Antarctic Ice Sheet retreat driven by Holocene warm water incursions, *Nature* 547, 43-48  
670 <https://doi.org/10.1038/nature22995>, 2017.

671 Ho, S. L., Mollenhauer, G., Feitz, S., Martinez-Garcia, A., Lamy, F., Rueda, G., Schipper, K., Méheust, M.,  
672 Rosell-Melé, Stein, R. and Tiedemann, R.: Appraisal of TEX86 and TEX86L thermometries in subpolar and  
673 polar regions, *Geochim. Cosmochim. Acta.*, 131, 213-226, <https://doi.org/10.1016/j.gca.2014.01.001>, 2014.

674 Ho, S. L., Yamamoto, M., Mollenhauer, G. and Minagawa, M.: Core top TEX86 values in the South and  
675 equatorial Pacific, *Org. Geochem.*, 42, 94-99, <https://doi.org/10.1016/j.orggeochem.2010.10.012>, 2011.

676 Hu, A. Y., Jiao, N. Z., Zhang, R. and Yang, Z.: Niche partitioning of marine group I Crenarchaeota in the  
677 euphotic and upper mesopelagic zones of the East China Sea, *Appl. Environ. Microbiol.*, 77, 7469–7478,  
678 <https://doi.org/10.1128/Aem.00294-11>, 2011.

679 Huguet, C. Kim, J.-H., Sinninghe Damsté, J.S. and Schouten, S.: Reconstruction of sea surface temperature  
680 variations in the Arabian Sea over the last 23 kyr using organic proxies (TEX86 and U37K'), *Paleoceanogr.*  
681 *Paleoclimatol.*, 21, PA3003, <https://doi.org/10.1029/2005PA001215>, 2006.

682 Huguet, C., Urakawa, H., Martens-Habbena, W., Truxal, L., Stahl, D. A. and Ingalls, A. E.: Changes in intact  
683 membrane lipid content of archaeal cells as an indication of metabolic status, *Org. Geochem.*, 41, 930–934,  
684 <https://doi.org/10.1016/j.orggeochem.2010.04.012>, 2010.

685 Huguet, C., Martrat, B., Grimalt, J.O., Sinninghe Damsté, J.S. and Schouten, S.: Coherent millennial-scale  
686 patterns in U37k' and TEX86H temperature records during the penultimate interglacial-to-glacial cycle in the  
687 western Mediterranean, 26, PA2218, <https://doi.org/10.1029/2010PA002048>, 2011.

688 Huguet, C., Fietz, S. and Rosell-Melé, A.: Global distribution patterns of hydroxy glycerol dialkyl glycerol  
689 tetraethers, *Org. Geochem.*, 57, 107–118, <https://doi.org/10.1016/j.orggeochem.2013.01.010>, 2013.

690 Huguet, C., Fietz, S., Rosell-Mele, A., Daura, X. and Costenaro, L.: Molecular dynamics simulation study of  
691 the effect of glycerol dialkyl glycerol tetraether hydroxylation on membrane thermostability, *Biochim.*  
692 *Biophys. Acta-Biomembr.*, 1859, 966–974, <https://doi.org/10.1016/j.bbamem.2017.02.009>, 2017.

693 Hurley, S. J., Lipp, J. S., Close, H. G., Hinrichs, K. U. and Pearson, A.: Distribution and export of isoprenoid  
694 tetraether lipids in suspended particulate matter from the water column of the Western Atlantic Ocean, *Org.*  
695 *Geochem.*, 116, 90–102, <https://doi.org/10.1016/j.orggeochem.2017.11.010>, 2018.

696 Ingalls, A. E., Shah, S. R., Hansman, R. L., Aluwihare, L. I., Santos, G. H., Druffel, E. R. M. and Pearson,  
697 A.: Quantifying archaeal community autotrophy in the mesopelagic ocean using natural radiocarbon, PNAS,  
698 103, 6442-6447, [https://doi.org/ 10.1073/pnas.0510157103](https://doi.org/10.1073/pnas.0510157103), 2006.

699 Ingalls, A. E., Huguet, C. and Truxal, L.: Distribution of Intact and Core Membrane Lipids of Archaeal  
700 Glycerol Dialkyl Glycerol Tetraethers among Size-Fractionated Particulate Organic Matter in Hood Canal,  
701 Puget Sound, Appl. Environ. Microbiol., 78, 1480-1490, [https://doi.org/ 10.1128/AEM.07016-11](https://doi.org/10.1128/AEM.07016-11), 2012.

702 Jacobs, S. S., Hellmer, H. H. and Jenkins, A.: Antarctic ice sheet melting in the Southeast Pacific, Geophys.  
703 Res. Lett., 23, 957-960, <https://doi.org/10.1029/96gl00723>, 1996.

704 Jacobs, S. S., Jenkins, A., Giulivi, C. F. and Dutrieux, P.: Stronger ocean circulation and increased melting  
705 under Pine Island Glacier ice shelf, Nat. Geosci., 4, 519-523, <https://doi.org/10.1038/ngeo1188>, 2011.

706 Jenkins, A., Dutrieux, P., Jacobs, S. S., McPhail, S. D., Perrett, J. R., Webb, A. T. and White, D.:  
707 Observations beneath Pine Island Glacier in West Antarctica and implications for its retreat, Nat. Geosci., 3,  
708 468-472, <https://doi.org/10.1038/ngeo890>, 2010.

709 Jenkyns, H.C., Forster, A., Schouten, S. and Sinninghe Damsté, J.S.: High temperatures in the Late  
710 Cretaceous Arctic Ocean, Nature, 432, 888-892, [https://doi.org/ 10.1038/nature03143](https://doi.org/10.1038/nature03143), 2004.

711 Joughin, I., Smith, B. E. and Medley, B.: Marine ice sheet collapse potentially under way for the Thwaites  
712 Glacier Basin, West Antarctica, Science, 344, 735-738, <https://doi.org/10.1126/science.1249055>, 2014.

713 Kalanetra, K. M., Bano, N. and Hollibaugh, J. T.: Ammonia-oxidizing archaea in the Arctic Ocean and  
714 Antarctic coastal waters, Environ. Microbiol., 11, 2434-2445, <https://doi.org/10.1111/j.1462->  
715 2920.2009.01974.x, 2009.

716 Kang, S. J., Shin, K. H. and Kim, J. H.: Occurrence and distribution of hydroxylated isoprenoid glycerol  
717 dialkyl glycerol tetraethers (OH-GDGTs) in the Han River system, South Korea, Acta Geochim., 36, 367-  
718 369, <https://doi.org/10.1007/s11631-017-0165-3>, 2017.

719 Kim, J.-G., Park, S.-J., Quan, Z.-X., Jung, M.-Y., Cha, I.-T., Kim, S.-J., Kim, K.-H., Yang, E.-J., Kim, Y.-N.,  
720 Lee, S.-H. and Rhee, S.-K.: Unveiling abundance and distribution of planktonic bacteria and archaea in a  
721 polynya in Amundsen Sea, Antarctica, Environ. Microbiol., 16, 1566-1578, [https://doi.org/ 10.1111/1462-](https://doi.org/10.1111/1462-)  
722 2920.12287. 2014.

723 Kim, J. -H., Schouten, S., Hopmans, E. C., Donner, B. and Sinninghe Damsté, J. S.: Global sediment core-  
724 top calibration of the TEX86 paleothermometer in the ocean, *Geochim. Cosmochim. Acta*, 72, 1154–1173,  
725 <https://doi.org/10.1016/i.gca.2007.12.010>, 2008.

726 Kim, J. -H., van der Meer, J., Schouten, S., Helmke, P., Willmott, V., Sangiorgi, F., Koç, N., Hopmans, E. C.  
727 and Sinninghe Damsté, J. S.: New indices and calibrations derived from the distribution of crenarchaeal  
728 isoprenoid tetraether lipids: Implications for past sea surface temperature reconstructions, *Geochim.*  
729 *Cosmochim. Acta*, 74, 4639–4654, <https://doi.org/10.1016/j.gca.2010.05.027>, 2010.

730 Kim, J.-H., Crosta, X., Willmott, V., Renssen, H., Bonnin, J., Helmke, P., Schouten, S. and Sinninghe  
731 Damsté, J. S.: Holocene subsurface temperature variability in the eastern Antarctic continental margin,  
732 *Geophys. Res. Lett.*, 39, n/a-n/a, <https://doi.org/10.1029/2012gl051157>, 2012.

733 Kim, J.-H., Villanueva, L., Zell, C. and Sinninghe Damsté, J. S.: Biological source and provenance of deep-  
734 water derived isoprenoid tetraether lipids along the Portuguese continental margin, *Geochim. Cosmochim.*  
735 *Acta*, 172, 177–204, <https://doi.org/10.1016/j.gca.2015.09.010>, 2016.

736 Kirchman, D. L., Elifantz, H., Dittel, A. I., Malmstrom, R. R. and Cottrell, M. T.: Standing stocks and  
737 activity of Archaea and Bacteria in the western Arctic Ocean, *Limnol. Oceanogr.*, 52, 495–507,  
738 <https://doi.org/10.4319/lo.2007.52.2.0495>, 2007.

739 Lee, S. H., Kang, Y-C. and Fuhrman, J. A.: Imperfect retention of natural bacterioplankton cells by glass  
740 fiber filters, *Mar. Ecol. Prog. Ser.*, 119, 285-290, <https://doi.org/10.3354/meps119285>, 1995.

741 Legendre, P., Oksanen, J. and ter Braak, C.J.: Testing the significance of canonical axes in redundancy  
742 analysis, *Methods Ecol. Evol.*, 2, 269-277, <https://doi.org/10.1111/j.2041-210X.2010.00078.x>, 2011.

743 Legendre, P. and Legendre, L.: *Numerical Ecology*, Third Edition, Elsevier, Oxford (UK), ISBN: 978-0-444-  
744 53869-7, 2012.

745 Lengger, S.K., Hopmans, E.C., Sinninghe Damsté, J.S. & Schouten, S.: Comparison of extraction and work  
746 up techniques for analysis of core and intact polar tetraether lipids from sedimentary environments. *Org.*  
747 *Geochem.* 47, 34-40, <http://doi.org/10.1016/j.orggeochem.2012.02.009>, 2012. Lengger, S. K., Kraaij, M.,  
748 Tjallingii, R., Baas, M., Stuut, J.-B., Hopmans, E. C., Sinninghe Damsté, J. S. and Schouten, S.: Differential

749 degradation of intact polar and core glycerol dialkyl glycerol tetraether lipids upon post-depositional  
750 oxidation, *Org. Geochem.*, 65, 83–93, <https://doi.org/https:10.1016/j.orggeochem.2013.10.004>, 2013.

751 Lengger, S. K., Hopmans, E. C., Sinninghe Damsté, J. S. and Schouten, S.: Fossilization and degradation of  
752 archaeal intact polar tetraether lipids in deeply buried marine sediments (Peru Margin), *Geobiology*, 12, 212–  
753 220, <https://doi.org/10.1111/gbi.12081>, 2014.

754 Lincoln, S. A., Wai, B., Eppley, J. M., Church, M. J., Summons, R. E. and DeLong, E. F.: Planktonic  
755 Euryarchaeota are a significant source of archaeal tetraether lipids in the ocean, *Proc. Natl. Acad. Sci. U. S.*  
756 *A.*, 111, 9858–9863, <https://doi.org/10.1073/pnas.1409439111>, 2014a.

757 Lincoln, S. A., Wai, B., Eppley, J. M., Church, M. J., Summons, R. E. and DeLong, E. F.: Reply to Schouten  
758 et al.: Marine Group II planktonic Euryarchaeota are significant contributors to tetraether lipids in the ocean,  
759 *Proc. Natl. Acad. Sci. U. S. A.*, 111, E4286–E4286, <https://doi.org/10.1073/pnas.1416736111>, 2014b.

760 Lipp, J. S. and Hinrichs, K. U.: Structural diversity and fate of intact polar lipids in marine sediments,  
761 *Geochim. Cosmochim. Acta*, 73, 6816–6833, <https://doi.org/10.1016/j.gca.2009.08.003>, 2009.

762 Lipp, J. S., Morono, Y., Inagaki, F. and Hinrichs, K. U.: Significant contribution of Archaea to extant  
763 biomass in marine subsurface sediments, *Nature*, 454, 991–994, <https://doi.org/10.1038/nature07174>, 2008.

764 Liu, X. L., Lipp, J. S., Simpson, J. H., Lin, Y. S., Summons, R. E. and Hinrichs, K. U.: Mono- and  
765 dihydroxyl glycerol dibiphytanyl glycerol tetraethers in marine sediments: Identification of both core and  
766 intact polar lipid forms, *Geochim. Cosmochim. Acta*, 89, 102–115,  
767 <https://doi.org/10.1016/j.gca.2012.04.053>, 2012.

768 Locarnini, R. A., Whitworth, T. and Nowlin, W. D.: The importance of the Scotia Sea on the outflow of  
769 Weddell Sea Deep-Water, *J. Mar. Res.*, 51, 135–153, <https://doi.org/10.1357/0022240933223846>, 1993.

770 Lu, X. X., Liu, X. L., Elling, F. J., Yang, H., Xie, S. C., Song, J. M., Li, X. G., Yuan, H. M., Li, N. and  
771 Hinrichs, K. U.: Hydroxylated isoprenoid GDGTs in Chinese coastal seas and their potential as a  
772 paleotemperature proxy for mid-to-low latitude marginal seas, *Org. Geochem.*, 89–90, 31–43,  
773 <https://doi.org/10.1016/j.orggeochem.2015.10.004>, 2015.

774 Luo, H. W., Tolar, B. B., Swan, B. K., Zhang, C. L. L., Stepanauskas, R., Moran, M. A. and Hollibaugh, J.  
775 T.: Single-cell genomics shedding light on marine Thaumarchaeota diversification, *Isme J.*, 8, 732–736,  
776 <https://doi.org/10.1038/ismej.2013.202>, 2014.

777 Mankoff, K. D., Jacobs, S. S., Tulaczyk, S. M. and Stammerjohn, S. E.: The role of Pine Island Glacier ice  
778 shelf basal channels in deep-water upwelling, polynyas and ocean circulation in Pine Island Bay, Antarctica,  
779 *Ann. Glaciol.*, 53, 123–128, <https://doi.org/10.3189/2012AoG60A062>, 2012.

780 Massana, R., Taylor, L. J., Murray, A. E., Wu, K. Y., Jeffrey, W. H. and DeLong, E. F.: Vertical distribution  
781 and temporal variation of marine planktonic archaea in the Gerlache Strait, Antarctica, during early spring,  
782 *Limnol. Oceanogr.*, 43, 607–617, <https://doi.org/10.4319/lo.1998.43.4.0607>, 1998.

783 Menviel, L., Timmermann, A., Timm, O. E. and Mouchet, A.: Climate and biogeochemical response to a  
784 rapid melting of the West Antarctic Ice Sheet during interglacials and implications for future climate,  
785 *Paleoceanography*, 25, <https://doi.org/10.1029/2009PA001892>, 2010.

786 Merbt, S. N., Stahl, D. A., Casamayor, E. O., Marti, E., Nicol, G. W. and Prosser, J. I.: Differential  
787 photoinhibition of bacterial and archaeal ammonia oxidation, *Fems Microbiol. Lett.*, 327, 41–46,  
788 <https://doi.org/10.1111/j.1574-6968.2011.02457.x>, 2012.

789 Meredith, M. P., Naveira Garabato, A. C., Stevens, D. P., Heywood, K. J., and Sanders, R. J.: Deep and  
790 Bottom Waters in the Eastern Scotia Sea: Rapid Changes in Properties and Circulation, *J. Phys. Oceanogr.*,  
791 31, 2157–2168, [https://doi.org/10.1175/1520-0485\(2001\)031<2157:DABWIT>2.0.CO;2](https://doi.org/10.1175/1520-0485(2001)031<2157:DABWIT>2.0.CO;2), 2001.

792 Mincer, T. J., Church, M. J., Taylor, L. T., Preston, C., Kar, D. M. and DeLong, E. F.: Quantitative  
793 distribution of presumptive archaeal and bacterial nitrifiers in Monterey Bay and the North Pacific  
794 Subtropical Gyre, *Environ. Microbiol.*, 9, 1162–1175, <https://doi.org/10.1111/j.1462-2920.2007.01239.x>,  
795 2007.

796 Mougnot, J., Rignot, E. and Scheuchl, B.: Sustained increase in ice discharge from the Amundsen Sea  
797 Embayment, West Antarctica, from 1973 to 2013, *Geophys. Res. Lett.*, 41, 1576–1584, <https://doi.org/10.1002/2013GL059069>, 2014.

799 Murray, A. E., Preston, C. M., Massana, R., Taylor, L. T., Blakis, A., Wu, K. and DeLong, E. F.: Seasonal  
800 and spatial variability of bacterial and archaeal assemblages in the coastal waters near Anvers Island,  
801 Antarctica, *Appl. Environ. Microbiol.*, 64, 2585–2595, [https://doi.org/ 10.1128/AEM.64.7.2585-2595](https://doi.org/10.1128/AEM.64.7.2585-2595), 1998.

802 Naveira Garabato, A. C., Heywood, K. J. and Stevens, D. P.: Modification and pathways of Southern Ocean  
803 Deep Waters in the Scotia Sea, *Deep Sea Res. Part I Oceanogr. Res. Pap.*, 49, 681-705, [https://doi.org/](https://doi.org/10.1016/S0967-0637(01)00071-1)  
804 [10.1016/S0967-0637\(01\)00071-1](https://doi.org/10.1016/S0967-0637(01)00071-1), 2002a.

805 Naveira Garabato, A. C., Strass, V. H. and Kattner, G.: Fluxes of nutrients in a three-dimensional meander  
806 structure of the Antarctic Polar Front, *Deep Sea Res. Part II Top. Stud. Oceanogr.*, 49, 3771-3792,  
807 [https://doi.org/10.1016/S0967-0645\(02\)00110-8](https://doi.org/10.1016/S0967-0645(02)00110-8), 2002b.

808 Orsi, A. H., Whitworth, T. and Nowlin Jr., W. D.: On the meridional extent and fronts of the Antarctic  
809 Circumpolar Current, *Deep Sea Res. Part I Oceanogr. Res. Pap.*, 42, 641-673, [https://doi.org/10.1016/0967-](https://doi.org/10.1016/0967-0637(95)00021-W)  
810 [0637\(95\)00021-W](https://doi.org/10.1016/0967-0637(95)00021-W), 1995.

811 Paolo, F. S., Fricker, H. A. and Padman, L.: Volume loss from Antarctic ice shelves is accelerating, *Science*,  
812 348, 327-331, <https://doi.org/10.1126/science.aaa0940>, 2015.

813 Park, J., Kuzminov, F. I., Bailleul, B., Yang, E. J., Lee, S., Falkowski, P. G. and Gorbunov, M. Y.: Light  
814 availability rather than Fe controls the magnitude of massive phytoplankton bloom in the Amundsen Sea  
815 polynyas, *Antarctica, Limnol. Oceanogr.*, 62, 2260–2276, <https://doi.org/10.1002/lno.10565>, 2017.

816 Pitcher, A., Hopmans, E.C., Schouten, S. & Sinninghe Damste, J.S.: Separation of core and intact polar  
817 archaeal tetraether lipids using silica columns: Insights into living and fossil biomass contributions, *Org.*  
818 *Geochem.* 40, 12-19, <http://doi.org/10.1016/j.orggeochem.2008.09.008>, 2009.

819 Pitcher, A., Rychlik, N., Hopmans, E. C., Spieck, E., Rijpstra, W. I. C., Ossebaar, J., Schouten, S., Wagner,  
820 M. and Sinninghe Damsté, J. S.: Crenarchaeol dominates the membrane lipids of “*Candidatus*  
821 *Nitrososphaera gargensis*”, a thermophilic Group I. 1b Archaeon, *Isme J.*, 4, 542–552,  
822 <https://doi.org/10.1038/ismej.2009.138>, 2010.

823 Pitcher, A., Hopmans, E. C., Mosier, A. C., Park, S. J., Rhee, S. K., Francis, C. A., Schouten, S. and  
824 Sinninghe Damsté, J. S.: Core and Intact Polar Glycerol Dibiphytanyl Glycerol Tetraether Lipids of

825 Ammonia-Oxidizing Archaea Enriched from Marine and Estuarine Sediments, *Appl. Environ. Microbiol.*,  
826 77, 3468–3477, <https://doi.org/10.1128/Aem.02758-10>, 2011.

827 Pritchard, H. D., Arthern, R. J., Vaughan, D. G. and Edwards, L. A.: Extensive dynamic thinning on the  
828 margins of the Greenland and Antarctic ice sheets, *Nature*, 461, 971–975,  
829 <https://doi.org/10.1038/nature08471>, 2009.

830 Raes, E. J., Bodrossy, L., van de Kamp, J., Bissett, A., Ostrowski, M., Brown, M. V., Sow, S. L. S., Sloyan,  
831 B. and Waite, A. M.: Oceanographic boundaries constrain microbial diversity gradients in the South Pacific  
832 Ocean, *Proc. Natl. Acad. Sci.*, 115, E8266–E8275, <https://doi.org/10.1073/pnas.1719335115>, 2018.

833 Raiswell, R., Benning, L. G., Tranter, M. and Tulaczyk, S.: Bioavailable iron in the Southern Ocean: the  
834 significance of the iceberg conveyor belt, *Geochem. Trans.*, 9, <https://doi.org/10.1186/1467-4866-9-7>, 2008.

835 Rignot, E. and Jacobs, S. S.: Rapid bottom melting widespread near Antarctic ice sheet grounding lines,  
836 *Science*, 296, 2020–2023, <https://doi.org/10.1126/science.1070942>, 2002.

837 Rignot, E., Bamber, J. L., Van Den Broeke, M. R., Davis, C., Li, Y. H., Van De Berg, W. J. and Van  
838 Meijgaard, E.: Recent Antarctic ice mass loss from radar interferometry and regional climate modelling, *Nat.*  
839 *Geosci.*, 1, 106–110, <https://doi.org/10.1038/ngeo102>, 2008.

840 Rignot, E., Jacobs, S., Mouginot, J. and Scheuchl, B.: Ice-Shelf Melting Around Antarctica, *Science*, 341,  
841 266–270, <https://doi.org/10.1126/science.1235798>, 2013.

842 Rignot, E., Mouginot, J., Scheuchl, B., Van Den Broeke, M., Van Wessem, M.J. and Morlighem, M.: Four  
843 decades of Antarctic ice sheet mass balance from 1979-2017, *PNAS*, 116, 1095-1103, <https://doi.org/10.1073/pnas.1812883116>, 2019.

845 Rubin, S. I.: Carbon and nutrient cycling in the upper water column across the Polar Frontal Zone and  
846 Antarctic Circumpolar Current along 170°W, *Glob. Biogeochem. Cycles*, 17, 1-14,  
847 <https://doi.org/10.1029/2002GB001900>, 2003.

848 Schouten, S., Hopmans, E. C., Pancost, R. D. and Sinninghe Damsté, J. S.: Widespread occurrence of  
849 structurally diverse tetraether membrane lipids: Evidence for the ubiquitous presence of low-temperature  
850 relatives of hyperthermophiles, *Proc. Natl. Acad. Sci. U. S. A.*, 97, 14421–14426,  
851 <https://doi.org/10.1073/pnas.97.26.14421>, 2000.

852 Schouten, S., Hopmans, E. C., Schefuß, E. and Sinninghe Damsté, J. S.: Distributional variations in marine  
853 crenarchaeotal membrane lipids: a new tool for reconstructing ancient sea water temperatures?, *Earth Planet.*  
854 *Sci. Lett.*, 204, 265–274, [https://doi.org/10.1016/S0012-821X\(02\)00979-2](https://doi.org/10.1016/S0012-821X(02)00979-2), 2002.

855 Schouten, S., Hopmans, E.C., Rosell-Melé, A., Pearson, A., Adam, P., Bauersachs, T., Bard, E., Bernasconi,  
856 S.M., Bianchi, T.S., Brocks, J.J., Carlson, L.T., Castañeda, I.S., Derenne, S., Selver, A.D., Dutta, K.,  
857 Eglinton, T., Fosse, C., Galy, V., Grice, K., Hinrichs, K.U., Huang, Y., Huguet, A., Huguet, C., Hurley, S.,  
858 Ingalls, A., Jia, G., Keely, B., Knappy, C., Kondo, M., Krishnan, S., Lincoln, S., Lipp, J., Mangelsdorf, K.,  
859 Martínez-García, A., Ménot, G., Mets, A., Mollenhauer, G., Ohkouchi, N., Ossebaar, J., Pagani, M., Pancost,  
860 R.D., Pearson, E.J., Peterse, F., Reichart, G.J., Schaeffer, P., Schmitt, G., Schwark, L., Shah, S.R., Smith,  
861 R.W., Smittenberg, R.H., Summons, R.E., Takano, Y., Talbot, H.M., Taylor, K.W.R., Tarozo, R., Uchida,  
862 M., Van Dongen, B.E., Van Mooy, B.A.S., Wang, J., Warren, C., Weijers, J.W.H., Werne, J.P., Woltering,  
863 M., Xie, S., Yamamoto, M., Yang, H., Zhang, C.L., Zhang, Y., Zhao, M. & Sinninghe Damsté, J.S.: An  
864 interlaboratory study of TEX86 and BIT analysis of sediments, extracts, and standard mixtures, *Geochem.*  
865 *Geophys. Geosyst.*, 14, 5263-5265, <https://doi.org/10.1002/2013GC004904>, 2013.

866 Schouten, S., Huguet, C., Hopmans, E. C., Kienhuis, M. V. M. and Sinninghe Damsté, J. S.: Analytical  
867 methodology for TEX86 paleothermometry by high-performance liquid chromatography/atmospheric  
868 pressure chemical ionization-mass spectrometry, *Anal. Chem.*, 79, 2940–2944,  
869 <https://doi.org/10.1021/ac062339v>, 2007.

870 Schouten, S., Baas, M., Hopmans, E. C., Reysenbach, A. L. and Sinninghe Damsté, J. S.: Tetraether  
871 membrane lipids of *Candidatus “Aciduliprofundum boonei”*, a cultivated obligate thermoacidophilic  
872 euryarchaeote from deep-sea hydrothermal vents, *Extremophiles*, 12, 119–124,  
873 <https://doi.org/10.1007/s00792-007-0111-0>, 2008.

874 Schouten, S., Middelburg, J. J., Hopmans, E. C. and Sinninghe Damsté, J. S.: Fossilization and degradation  
875 of intact polar lipids in deep subsurface sediments: A theoretical approach, *Geochim. Cosmochim. Acta*, 74,  
876 3806–3814, <https://doi.org/10.1016/j.gca.2010.03.029>, 2010.

877 Schouten, S., Pitcher, A., Hopmans, E. C., Villanueva, L., van Bleijswijk, J. and Sinninghe Damsté, J. S.:  
878 Intact polar and core glycerol dibiphytanyl glycerol tetraether lipids in the Arabian Sea oxygen minimum



879 zone: I. Selective preservation and degradation in the water column and consequences for the TEX86,  
880 *Geochim. Cosmochim. Acta*, 98, 228–243, <https://doi.org/10.1016/j.gca.2012.05.002>, 2012.

881 Schouten, S., Hopmans, E. C. and Sinninghe Damsté, J. S.: The organic geochemistry of glycerol dialkyl  
882 glycerol tetraether lipids: A review, *Org. Geochem.*, 54, 19–61,  
883 <https://doi.org/10.1016/j.orggeochem.2012.09.006>, 2013.

884 Schouten, S., Villanueva, L., Hopmans, E. C., van der Meer, M. T. J. and Sinninghe Damsté, J. S.: Are  
885 Marine Group II Euryarchaeota significant contributors to tetraether lipids in the ocean?, *Proc. Natl. Acad.*  
886 *Sci. U. S. A.*, 111, 4285, <https://doi.org/10.1073/pnas.1416176111>, 2014. Schubotz, F., Wakeham, S. G.,  
887 Lipp, J. S., Fredricks, H. F. and Hinrichs, K. U.: Detection of microbial biomass by intact polar membrane  
888 lipid analysis in the water column and surface sediments of the Black Sea, *Environ. Microbiol.*, 11, 2720–  
889 2734, <https://doi.org/10.1111/j.1462-2920.2009.01999.x>, 2009.

890 Shah, S. R., Mollenhauer, G., Ohkouchi, N., Eglinton, T. I. and Pearson, A.: Origins of archaeal tetraether  
891 lipids in sediments: Insights from radiocarbon analysis, *Geochim. Cosmochim. Acta.*, 72, 4577–4594,  
892 <https://doi.org/10.1016/j.gca.2008.06.021>, 2008.

893 Shepherd, A., Wingham, D. J., Mansley, J. A. D. and Corr, H. F. J.: Inland thinning of Pine Island Glacier,  
894 West Antarctica, *Science*, 291, 862–864, <https://doi.org/10.1126/science.291.5505.862>, 2001.

895 Shevenell, A.E., Ingalls, A.E., Dormack, E.W. and Kelly, C.: Holocene Southern Ocean surface temperature  
896 variability west of the Antarctic Peninsula. *Nature*, 470, 250–254, <https://doi.org/10.1038/nature09751>, 2011.

897 Signori, C.N., Pellizari, V.H., Enrich-Prast, A. and Sievert, S.M.: Spatiotemporal dynamics of marine  
898 bacterial and archaeal communities in surface waters off the northern Antarctic Peninsula, *Deep Sea Res.*  
899 *Part II Top. Stud. Oceanogr.*, 149, 150–160, <https://doi.org/10.1016/j.dsr2.2017.12.017>, 2018.

900 Sinninghe Damsté, J.S., van Bentum, E.C., Reichart, G-J., Pross, J. and Schouten, S.: A CO<sub>2</sub> decrease-driven  
901 cooling and increased latitudinal temperature gradient during the mid-Cretaceous Oceanic Anoxic Event 2,  
902 *Earth Planet. Sci. Lett.* 293, 97–103, <https://doi.org/10.1016/j.epsl.2010.02.027>, 2010.

903 Sinninghe Damsté, J. S., Rijpstra, W. I. C., Hopmans, E. C., Jung, M. Y., Kim, J. G., Rhee, S. K.,  
904 Stieglmeier, M. and Schleper, C.: Intact polar and core Glycerol Dibiphytanyl Glycerol Tetraether lipids of

905 Group I.1a and I.1b Thaumarchaeota in soil, *Appl. Environ. Microbiol.*, 78, 6866–6874,  
906 <https://doi.org/10.1128/aem.01681-12>, 2012.

907 Sinninghe Damsté, J. S., Rijpstra, W. I. C., Hopmans, E. C., den Uijl, M.J., Weijers, J.W.H., Schouten, S.  
908 The enigmatic structure of the crenarchaeol isomer, *Org. Geochem.*, 124, 22-28,  
909 <https://doi.org/10.1016/j.orggeochem.2018.06.005>, 2018.

910 Smith, J.A., Andersen, T.J., Shortt, M., Truffer, M., Stanton, T.P., Bindschadler, R., Dutrieux, P., Jenkins,  
911 A., Hillenbrand, C.-D., Ehrmann, W., Corr, H.F.J., Farley, N., Crowhurst, S. and Vaughan, D.G.: Sub-ice-  
912 shelf sediments record history of 20th Century retreat of Pine Island Glacier. *Nature* 540, 77-80,  
913 <https://doi.org/10.1038/nature20136>. 2017.

914 Sokolov, S. and Rintoul, S. R.: Circulation structure and distribution of the Antarctic Circumpolar Current  
915 fronts: 1. Mean circumpolar paths. *J. Geophys. Res.* 114, C11018, <https://doi.org/10.1029/2008JC005248>.  
916 2009.

917 Sollai, M., Villanueva, L., Hopmans, E.C., Reichart, G-J., Sinninghe Damsté, J.S.: A combined lipidomic  
918 and 16S rRNA gene amplicon sequencing approach reveals archaeal sources of intact polar lipids in the  
919 stratified Black Sea water column, *Geobiology.*, 17, 91-109, <https://doi.org/10.1111/gbi.12316>, 2019a.

920 Sollai, M., Villanueva, L., Hopmans, E.C., Keil, R.G., Sinninghe Damsté, J.S.: Archaeal sources of intact  
921 membrane lipid biomarkers in the oxygen deficient zone of the Eastern Tropical South Pacific, *Front.*  
922 *Microbiol.*, 10, <https://doi.org/10.3389/fmicb.2019.00765>, 2019b.

923 Sollich, M., Yoshinaga, M. Y., Hausler, S., Price, R. E., Hinrichs, K. U. and Buhning, S. I.: Heat stress  
924 dictates microbial lipid composition along a thermal gradient in marine sediments, *Front. Microbiol.*, 8, 1-19  
925 <https://doi.org/10.3389/fmicb.2017.01550>, 2017.

926 Spang, A., Hatzepichler, R., Brochier-Armanet, C., Rattei, T., Tischler, P., Spieck, E., Streit, W., Stahl, D.  
927 A., Wagner, M. and Schleper, C.: Distinct gene set in two different lineages of ammonia-oxidizing archaea  
928 supports the phylum Thaumarchaeota, *Trends Microbiol.*, 18, 331–340,  
929 <https://doi.org/10.1016/j.tim.2010.06.003>, 2010.

930 St-Laurent, P., Yager, P. L., Sherrell, R. M., Stammerjohn, S. E. and Dinniman, M. S.: Pathways and supply  
931 of dissolved iron in the Amundsen Sea (Antarctica), *J. Geophys. Res. Oceans*, 122, 7135–7162,  
932 <https://doi.org/10.1002/2017JC013162>, 2017.

933 Sturt, H. F., Summons, R. E., Smith, K., Elvert, M. and Hinrichs, K. U.: Intact polar membrane lipids in  
934 prokaryotes and sediments deciphered by high-performance liquid chromatography/electrospray ionization  
935 multistage mass spectrometry - new biomarkers for biogeochemistry and microbial ecology, *Rapid Commun.*  
936 *Mass Spectrom.*, 18, 617–628, <https://doi.org/10.1002/rcm.1378>, 2004.

937 Thuroczy, C.-E., Alderkamp, A.-C., Laan, P., Gerringa, L. J. A., Mills, M. M., Van Dijken, G. L., De Baar,  
938 H. J. W. and Arrigo, K. R.: Key role of organic complexation of iron in sustaining phytoplankton blooms in  
939 the Pine Island and Amundsen Polynyas (Southern Ocean), *Deep-Sea Res. Part II- Top. Stud. Oceanogr.*, 71–  
940 76, 49–60, <https://doi.org/10.1016/j.dsr2.2012.03.009>, 2012.

941 Tolar, B. B., Ross, M. J., Wallsgrove, N. J., Liu, Q., Aluwihare, L. I., Popp, B. N. and Hollibaugh, J. T.:  
942 Contribution of ammonia oxidation to chemoautotrophy in Antarctic coastal waters, *Isme J.*, 10, 2605–2619,  
943 <https://doi.org/10.1038/ismej.2016.61>, 2016.

944 Venables, H. J.: JR272A Weddell and Scotia Sea hydrographic section, British Antarctic Survey, Cambridge,  
945 UK, [https://www.bodc.ac.uk/resources/inventories/cruise\\_inventory/reports/jr272.pdf](https://www.bodc.ac.uk/resources/inventories/cruise_inventory/reports/jr272.pdf), 2012.

946 Vernet, M., Geibert, W., Hoppema, M., Brown, P. J., Haas, C., Hellmer, H. H., Jokat, W., Jullion, L.,  
947 Mazloff, M., Bakker, D. C. E., Brearley, J. A., Croot, P., Hattermann, T., Hauck, J., Hillenbrand, C.-D.,  
948 Hoppe, C. J. M., Huhn, O., Koch, B. P., Lechtenfeld, O. J., Meredith, M. P., Naveira Garabato, A. C.,  
949 Nöthig, E.-M., Peeken, I., Rutgers van der Loeff, M. M., Schmidtko, S., Schröder, M., Strass, V. H., Torres-  
950 Valdés, S. and Verdy, A.: The Weddell Gyre, Southern Ocean: Present knowledge and future challenges,  
951 *Rev. Geophys.* 57, 623-708, <https://doi.org/10.1029/2018RG000604>, 2019.

952 Wadham, J. L., De'ath, R., Monteiro, F. M., Tranter, M., Ridgwell, A., Raiswell, R. and Tulaczyk, S.: The  
953 potential role of the Antarctic Ice Sheet in global biogeochemical cycles, *Earth Environ. Sci. Trans. R. Soc.*  
954 *Edinb.*, 104, 55–67, <https://doi.org/10.1017/S1755691013000108>, 2013.

955 Wadham, J. L., Hawkings, J. R., Tarasov, L., Gregoire, L. J., Spencer, R. G. M., Gutjahr, M., Ridgwell, A.  
956 and Kohfeld, K. E.: Ice sheets matter for the global carbon cycle., *Nat. Commun.*, 10, 1-17, [https://doi.org/](https://doi.org/10.1038/s41467-019-11394-4)  
957 10.1038/s41467-019-11394-4, 2019.

958 Webber, B. G. M., Heywood, K. J., Stevens, D. P., Dutrieux, P., Abrahamsen, E. P., Jenkins, A., Jacobs, S.  
959 S., Ha, H. K., Lee, S. H., and Kim, T. W.: Mechanisms driving variability in the ocean forcing of Pine Island  
960 Glacier, *Nat. Commun.*, 8, [https://doi.org/ 14507](https://doi.org/14507), 10.1038/ncomms14507, 2017.

961 Weber, Y., Sinninghe Damsté, J.S., Hopmans, E.C., Lehmann, M.F. & Niemann, H.: Incomplete recovery of  
962 intact polar glycerol dialkyl glycerol tetraethers from lacustrine suspended biomass. *Limn. Oceanogr.*  
963 *Methods.* 15, 782-793. <http://10.1002/lom3.10198>. 2017.

964 Wilkins, D., Lauro, F. M., Williams, T. J., Demaere, M. Z., Brown, M. V., Hoffman, J. M., Andrews-  
965 Pfannkoch, C., Mcquaid, J. B., Riddle, M. J., Rintoul, S. R. and Cavicchioli, R.: Biogeographic partitioning  
966 of Southern Ocean microorganisms revealed by metagenomics, *Environ. Microbiol.*, 15, 1318–1333,  
967 <https://doi.org/10.1111/1462-2920.12035>, 2013.

968 Wingham, D. J., Wallis, D. W. and Shepherd, A.: Spatial and temporal evolution of Pine Island Glacier  
969 thinning, 1995-2006, *Geophys. Res. Lett.*, 36, 1-5, <https://doi.org/10.1029/2009gl039126>, 2009.

970 Xie, S. T., Lipp, J. S., Wegener, G., Ferdelman, T. G. and Hinrichs, K-U.: Turnover of microbial lipid in the  
971 deep biosphere and growth of benthic archaeal populations, *PNAS*, 100, 6010-6014, [https://doi.org/](https://doi.org/10.1073/pnas.1218569110)  
972 10.1073/pnas.1218569110, 2013.

973 Xie, S. T., Liu, X. L., Schubotz, F., Wakeham, S. G. and Hinrichs, K. U.: Distribution of glycerol ether lipids  
974 in the oxygen minimum zone of the Eastern Tropical North Pacific Ocean, *Org. Geochem.*, 71, 60–71,  
975 <https://doi.org/10.1016/j.orggeochem.2014.04.006>, 2014.

976 Yager, P.L., Sherrell, R.M., Stammerjohn, S.E., Alderkamp, A.-C., Schofield, O., Abrahamsen, E.P., Arrigo,  
977 K.R., Bertilsson, S., Garay, D.L., Guerrero, R., Lowry, K.E., Moksnes, P.-O., Ndungu, K., Post, A.F.,  
978 Randall-Goodwin, E., Riemann, L., Severmann, S., Thatje, S., van Dijken, G.L. and Wilson, S.: ASPIRE:  
979 The Amundsen sea Polynya international research expedition. *Oceanography*, 25, 40-53, [https://doi.org/](https://doi.org/10.5670/oceanog.2012.73)  
980 10.5670/oceanog.2012.73. 2012.

981 Zeng, Z., Liu, X-L., Farley, K. R., Wei, J. H., Metcalf, W. W., Summons, R. E. and Welander, P. V.: GDGT  
982 cyclization proteins identify the dominant archaeal sources of tetrarther lipids in the ocean. PNAS, 45,  
983 22505-22511, [https://doi.org/ 10.1073/pnas.1909306116](https://doi.org/10.1073/pnas.1909306116). 2019.

984 Zhang, Y. G., Pagani, M. and Zhengrong, W.: Ring Index: A new strategy to evaluate the integrity of TEX86  
985 paleothermometry. *Paleoceanography*, 31, 220-232, [https://doi.org/ 10.1002/2015PA002848](https://doi.org/10.1002/2015PA002848). 2016.

986 Zhu, C., Wakeham, S. G., Elling, F. J., Basse, A., Mollenhauer, G., Versteegh, G. J. M., Konneke, M. and  
987 Hinrichs, K. U.: Stratification of archaeal membrane lipids in the ocean and implications for adaptation and  
988 chemotaxonomy of planktonic archaea, *Environ. Microbiol.*, 18, 4324–4336, [https://doi.org/10.1111/1462-](https://doi.org/10.1111/1462-2920.13289)  
989 2920.13289, 2016.

990 Zwally, H. J., Giovinetto, M. B., Li, J., Cornejo, H. G., Beckley, M. A., Brenner, A. C., Saba, J. L. and Yi,  
991 D. H.: Mass changes of the Greenland and Antarctic ice sheets and shelves and contributions to sea-level  
992 rise: 1992-2002, *J. Glaciol.*, 51, 509–527, <https://doi.org/10.3189/172756505781829007>, 2005.

993 Table 1: Scotia Sea SPM samples studied and their physical properties including sample depth (m) and  
 994 sample layer where “M” denotes mixed layer and “T” denotes thermocline layer, GDGT-0/cren, and Ring  
 995 Index.

Latitude (°N)	Longitude (°E)	Station	Sample Depth (m)	Layer	Temperature (°C)	Salinity (PSU)	Fluorescence (ml/m <sup>3</sup> )	GDGT- 0/Cren	Ring Index
-53.013	-58.04	CTD 1	15	M	7.31	33.99	0.41	2.6	0.9
-53.013	-58.04	CTD 1	100	T	6.12	34.03	0.13	6.7	0.4
-53.586	-42.835	CTD 23	20	M	4.07	33.72	0.32		
-53.586	-42.835	CTD 23	100	T	2.23	33.81	0.08	1.8	0.7
-52.88	-41.787	CTD 24	15	M	3.55	33.72	1.09		
-52.88	-41.787	CTD 24	80	T	1.67	33.88	0.09	1.6	0.9
-53.743	-38.155	CTD 25	10	M	3.17	33.62	0.66		
-53.743	-38.155	CTD 25	80	T	1.95	33.91	0.05	2.4	0.8
-57.119	-31.815	CTD 22	30	M	1.34	33.82	0.24		
-56.167	-34.816	CTD 22	110	T	0.84	34.12	0.09	1.9	0.5
-57.459	-31.327	CTD 21	30	M	1.48	33.85	0.27		
-57.459	-31.327	CTD 21	110	T	1.34	34.3	0.03	5.3	0.2
-57.803	-30.83	CTD 20	30	M	1.60	33.92	0.28	2.2	1.0
-57.803	-30.83	CTD 20	110	T	1.01	34.15	0.06	6.8	0.2
-58.213	-30.822	CTD 19	20	M	1.29	33.9	0.27		
-58.213	-30.822	CTD 19	80	T	1.16	34.19	0.09	8.0	0.3
-58.624	-30.821	CTD 18	20	M	0.65	33.69	0.17		
-58.624	-30.821	CTD 18	90	T	-0.83	33.99	0.17	4.1	0.6
-59.436	-30.861	CTD 16	20	M	-0.64	33.67	0.17		
-59.436	-30.861	CTD 16	70	T	-1.32	34.12	0.08	16.8	1.0
-60.319	-30.961	CTD 13	30	M	-0.89	33.74	0.11		
-60.319	-30.961	CTD 13	65	T	-1.16	34.01	0.11	4.6	0.6
-61.171	-31.045	CTD 10	30	M	-1.08	33.82	0.15		
-61.171	-31.045	CTD 10	80	T	-1.08	34.23	0.11	177.6	0.02
-62.084	-31.174	CTD 7	40	M	-1.11	33.87	0.4		
-62.084	-31.174	CTD 7	75	T	-1.54	34.33	0.16	21.7	0.1
-62.784	-30.706	CTD 5	20	M	-1.13	33.87	0.28		
-62.784	-30.706	CTD 5	70	T	-1.49	34.34	0.14	4.3	0.7
-63.346	-29.569	CTD 3	20	M	-1.18	33.8	0.22		
-63.346	-29.569	CTD 3	60	T	-1.58	34.31	0.21	9.9	0.3

996

997 Table 2: Amundsen Sea SPM samples studied and their physical properties, GDGT-0/cren, and Ring Index.

Latitude (° N)	Longitude (°E)	Station	Sample Depth (m)	Temperature (°C)	Salinity (PSU)	Fluorescence (ml/m <sup>3</sup> )	GDGT- 0/Cren	Ring Index
-74.958	-101.829	PS104/003-1	10	-0.72	33.96	0.48	7.3	0.5
-74.958	-101.829	PS104/003-1	120	-1.19	34.13	0.01	4.8	0.5
-74.958	-101.829	PS104/003-1	180	-1.23	34.17	0.01	27.0	0.03
-74.958	-101.829	PS104/003-1	998	1.01	34.67	-0.02	4.8	0.7
-74.866	-100.76	PS104/007-1	20	-0.12	33.52	3.78	8.2	0.4
-74.866	-100.76	PS104/007-1	120	-0.91	34.08	0.01	4.9	0.5
-74.866	-100.76	PS104/007-1	240	-1.33	34.14	-0.01	5.0	0.4
-74.866	-100.76	PS104/007-1	685	0.87	34.63	-0.02	4.2	0.6
-74.359	-101.747	PS104/017-1	10	-0.17	33.42	7.89		
-74.359	-101.747	PS104/017-1	150	-1.61	34.16	0.01	5.8	0.3
-74.359	-101.747	PS104/017-1	1375	1.06	34.71	-0.02	2.8	0.9
-72.768	-107.093	PS104/022-1	10	-0.59	33.13	1.09		
-72.768	-107.093	PS104/022-1	30	-0.47	33.27	1.71		
-72.768	-107.093	PS104/022-1	120	-1.54	34.1	0.07	3.8	0.6
-72.768	-107.093	PS104/022-1	697	0.98	34.71	-0.02	4.2	0.6
-73.297	-112.328	PS104/043-2	10	-1.34	32.82	1.51		
-73.297	-112.328	PS104/043-2	120	-1.62	34.18	0.01	3.3	0.5
-73.297	-112.328	PS104/043-2	454	0.15	34.51	-0.02	5.4	0.5

998

999 Table 3: Relative abundances (%) and heat map of IPLs identified in Amundsen Sea. Relative abundances

1000 >30% indicated in red, low relative abundances <10% indicated in green. nd = not detected.

Station	Depth (cm)	GDGT-0			GDGT-1	GDGT-2	Crenarchaeol			OH-GDGT-0			diOH- GDGT-0
		MH	DH	HPH	DH	DH	MH	DH	HPH	MH	DH	HPH	MH
PS104/003-1	10	1.2	nd	81.8	nd	nd	0.2	nd	11.1	0.4	5.1	nd	0.2
PS104/003-1	120	0.6	2.2	56.2	1.5	nd	0.3	0.1	11.7	4.9	16.5	0.5	5.5
PS104/003-1	180	1.4	nd	18.0	nd	nd	0.7	nd	nd	24.1	25.7	nd	30.1
PS104/003-1	998	3.4	11.3	28.1	14.7	8.2	1.7	3.0	4.3	5.2	18.8	nd	1.3
PS104/007-1	20	89.1	nd	nd	nd	nd	10.9	nd	nd	nd	nd	nd	nd
PS104/007-1	120	1.4	4.6	38.8	5.1	1.9	1.0	0.4	7.7	6.9	25.7	nd	6.5
PS104/007-1	240	2.3	5.7	40.0	3.3	nd	1.3	nd	8.3	11.8	11.9	nd	15.4
PS104/007-1	685	1.3	8.9	37.8	9.1	4.1	1.3	1.8	8.3	3.6	22.7	nd	1.1
PS104/017-1	10	nd	nd	nd	nd	nd	nd	nd	nd	nd	nd	nd	nd
PS104/017-1	150	1.7	nd	43.9	nd	nd	1.0	nd	6.8	14.1	13.0	nd	19.5
PS104/017-1	1375	0.9	6.5	38.2	11.1	7.3	1.1	3.0	11.9	2.4	17.3	nd	0.3
PS104/022-1	10	nd	nd	nd	nd	nd	nd	nd	nd	nd	nd	nd	nd
PS104/022-1	30	nd	nd	nd	nd	nd	nd	nd	nd	nd	nd	nd	nd
PS104/022-1	120	2.8	nd	51.6	nd	nd	1.7	nd	12.4	11.1	9.3	1.2	9.9
PS104/022-1	697	4.3	6.0	31.5	11.2	5.3	2.0	2.3	5.6	5.5	25.0	nd	1.2
PS104/043-2	10	nd	nd	nd	nd	nd	nd	nd	nd	nd	nd	nd	nd
PS104/043-2	120	1.6	nd	38.3	nd	nd	0.5	nd	11.5	4.6	37.9	0.9	4.7
PS104/043-2	454	0.7	0.2	72.3	nd	nd	0.2	nd	13.2	1.7	8.6	0.7	2.4

1001



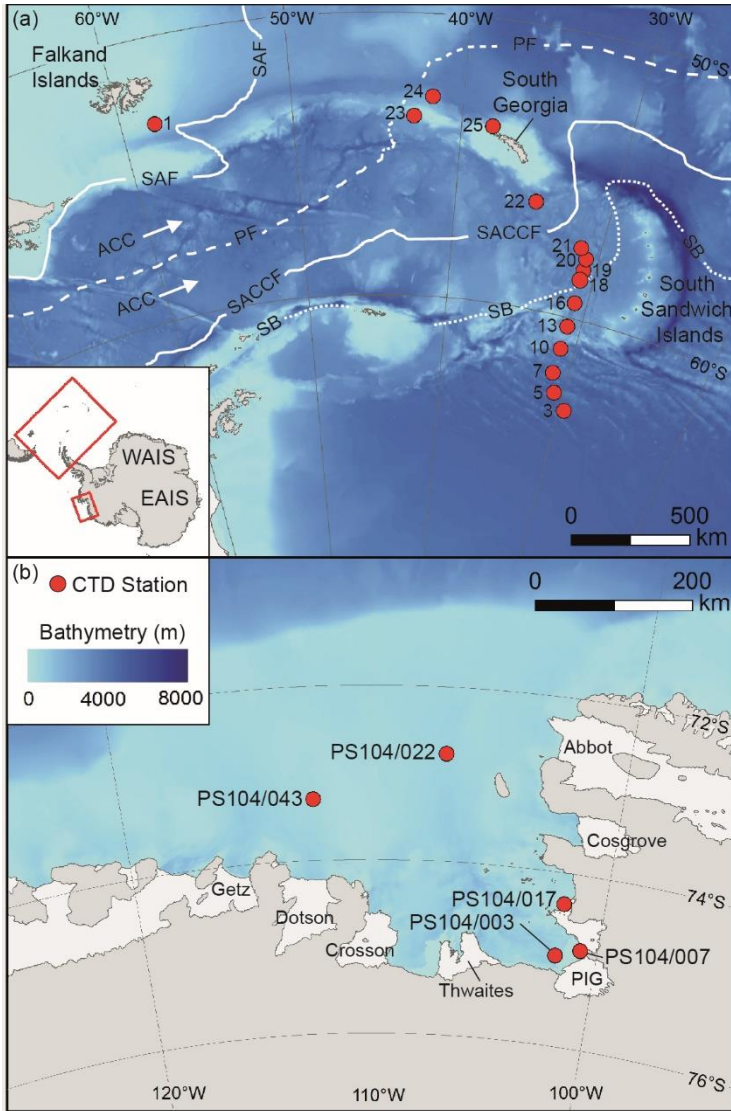
1002 Table 4: Relative abundances (%) and heat map of IPLs identified in Scotia Sea. Relative abundances >30%  
 1003 indicated in red, low relative abundances <10% indicated in green. nd = not detected.

CTD	Depth (m)	GDGT-0			GDGT-1	Crenarchaeol			OH-GDGT-0			diOH-GDGT-0
		MH	DH	HPH	DH	MH	DH	HPH	MH	DH	HPH	MH
1	15	6.8	nd	49.6	nd	3.4	nd	18.6	nd	21.6	nd	nd
1	100	4.6	nd	54.9	nd	3.3	nd	5.6	2.6	28.2	nd	0.8
23	20	nd	nd	nd	nd	nd	nd	nd	nd	nd	nd	nd
23	100	31.0	nd	nd	nd	16.8	nd	nd	19.6	17.7	nd	14.9
24	15	nd	nd	nd	nd	nd	nd	nd	nd	nd	nd	nd
24	80	36.2	nd	1.6	nd	23.3	nd	nd	16.5	15.7	nd	6.7
25	10	nd	nd	nd	nd	nd	nd	nd	nd	nd	nd	nd
25	80	10.1	1.0	35.3	nd	6.1	nd	13.4	8.7	14.8	1.8	8.8
22	30	nd	nd	nd	nd	nd	nd	nd	nd	nd	nd	nd
22	110	13.5	nd	8.8	nd	11.9	nd	nd	21.7	23.7	nd	20.4
21	30	52.6	nd	nd	nd	nd	nd	nd	47.4	nd	nd	nd
21	110	9.3	4.0	10.2	3.5	4.5	nd	nd	11.8	35.3	nd	21.4
20	30	53.0	nd	nd	nd	24.5	nd	nd	22.5	nd	nd	nd
20	110	9.0	nd	31.8	nd	6.0	nd	nd	12.4	28.2	nd	12.6
19	20	nd	nd	nd	nd	nd	nd	nd	nd	nd	nd	nd
19	80	3.1	nd	55.7	nd	2.6	nd	4.8	6.4	19.2	nd	8.2
18	20	nd	nd	nd	nd	nd	nd	nd	nd	nd	nd	nd
18	90	4.2	nd	57.8	nd	1.9	nd	13.4	4.7	9.2	2.6	6.2
16	20	nd	nd	100.0	nd	nd	nd	nd	nd	nd	nd	nd
16	70	7.8	nd	45.9	nd	3.2	nd	nd	20.6	8.9	nd	13.6
13	30	nd	nd	nd	nd	nd	nd	nd	nd	nd	nd	nd
13	65	15.3	nd	54.2	nd	4.1	nd	11.1	10.5	nd	nd	4.8
10	30	nd	nd	nd	nd	nd	nd	nd	nd	nd	nd	nd
10	80	4.2	nd	82.6	nd	0.5	nd	nd	7.0	nd	nd	5.7
7	40	nd	nd	nd	nd	nd	nd	nd	nd	nd	nd	nd
7	75	7.2	nd	47.7	nd	2.5	nd	nd	29.8	nd	nd	12.7
5	20	nd	nd	nd	nd	nd	nd	nd	nd	nd	nd	nd
5	70	0.7	nd	71.1	nd	0.4	nd	16.3	2.3	4.8	2.5	1.9
3	20	nd	nd	nd	nd	nd	nd	nd	nd	nd	nd	nd
3	60	45.2	nd	22.7	nd	6.9	nd	nd	25.2	nd	nd	nd

1004

1005

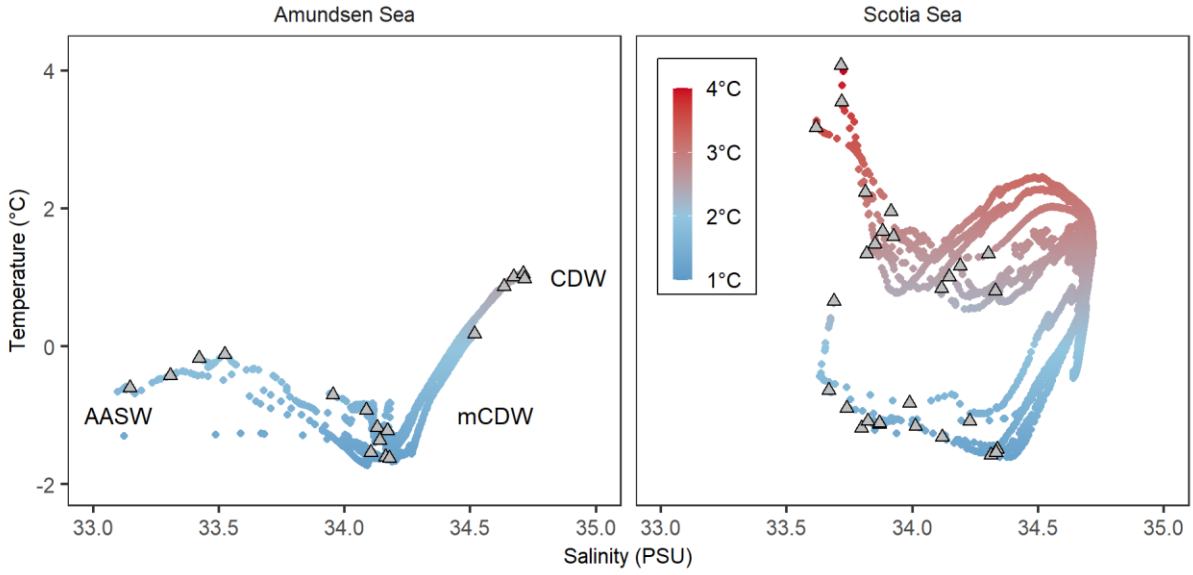
1006 Figure 1. Map showing studied CTD sampling stations (red dots) in the Scotia sea (A) and Amundsen sea  
 1007 (B). The main oceanic fronts are also shown in panel A; subantarctic (SAF), polar (PF), southern ACC  
 1008 (SACCF) and the southern boundary of the ACC (SB) (Sokolov and Rintoul, 2009). The names of the ice  
 1009 shelves are shown in panel B.



1010

1011

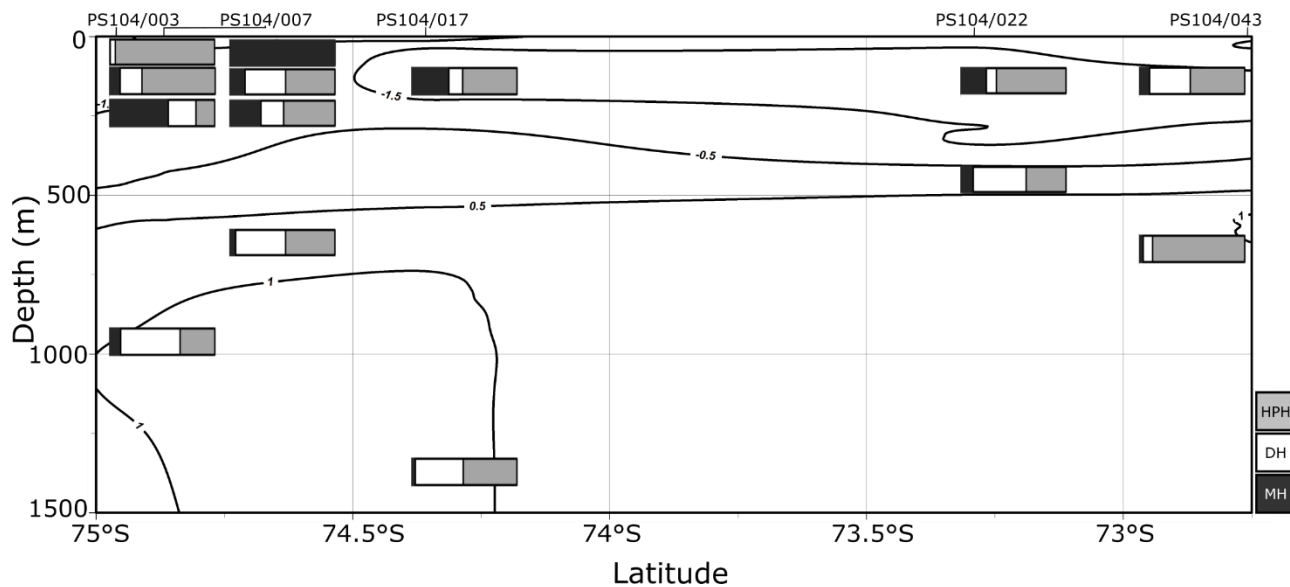
1012 Figure 2. The temperature and salinity profiles (T-S plot) for the Amundsen Sea (A) showing Antarctic  
1013 Surface Water (AASW) and Circumpolar Deep Water (CDW), and Scotia Sea (B). Coloured circles indicate  
1014 the water column temperature of the water masses with the grey triangles indicating the water column  
1015 sampling depths.



1016

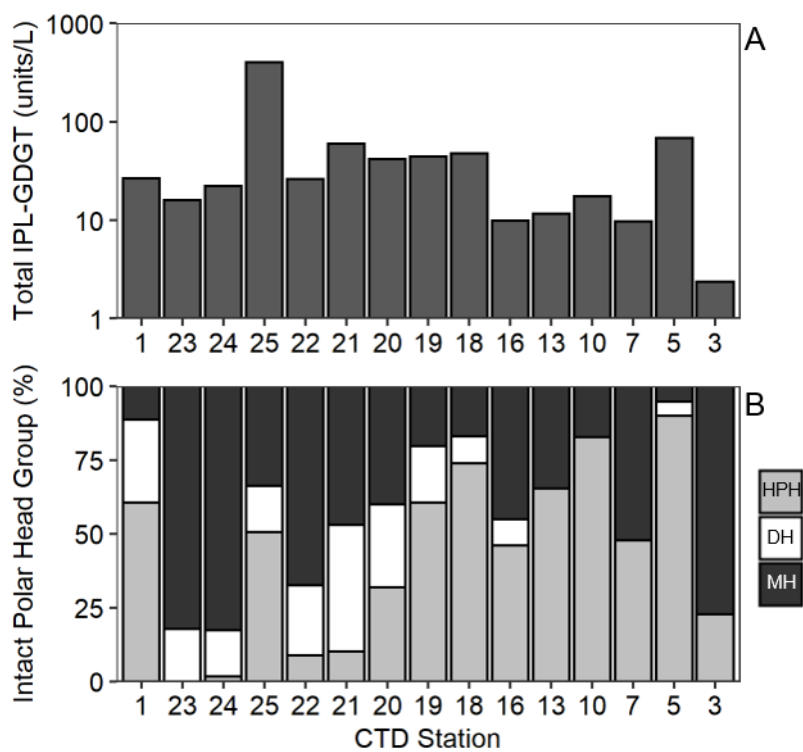
1017

1018 Figure 3. Relative abundance (%) of intact GDGTs at approximate sample depths in the Amundsen Sea. Bars  
1019 reflect intact-GDGT head group with black representing MH head groups, white representing DH, and grey  
1020 representing HPH. Contour lines show approximate ocean temperature ranges using CTD data taken at each  
1021 sample station with Ocean Data View DIVA gridding.



1022

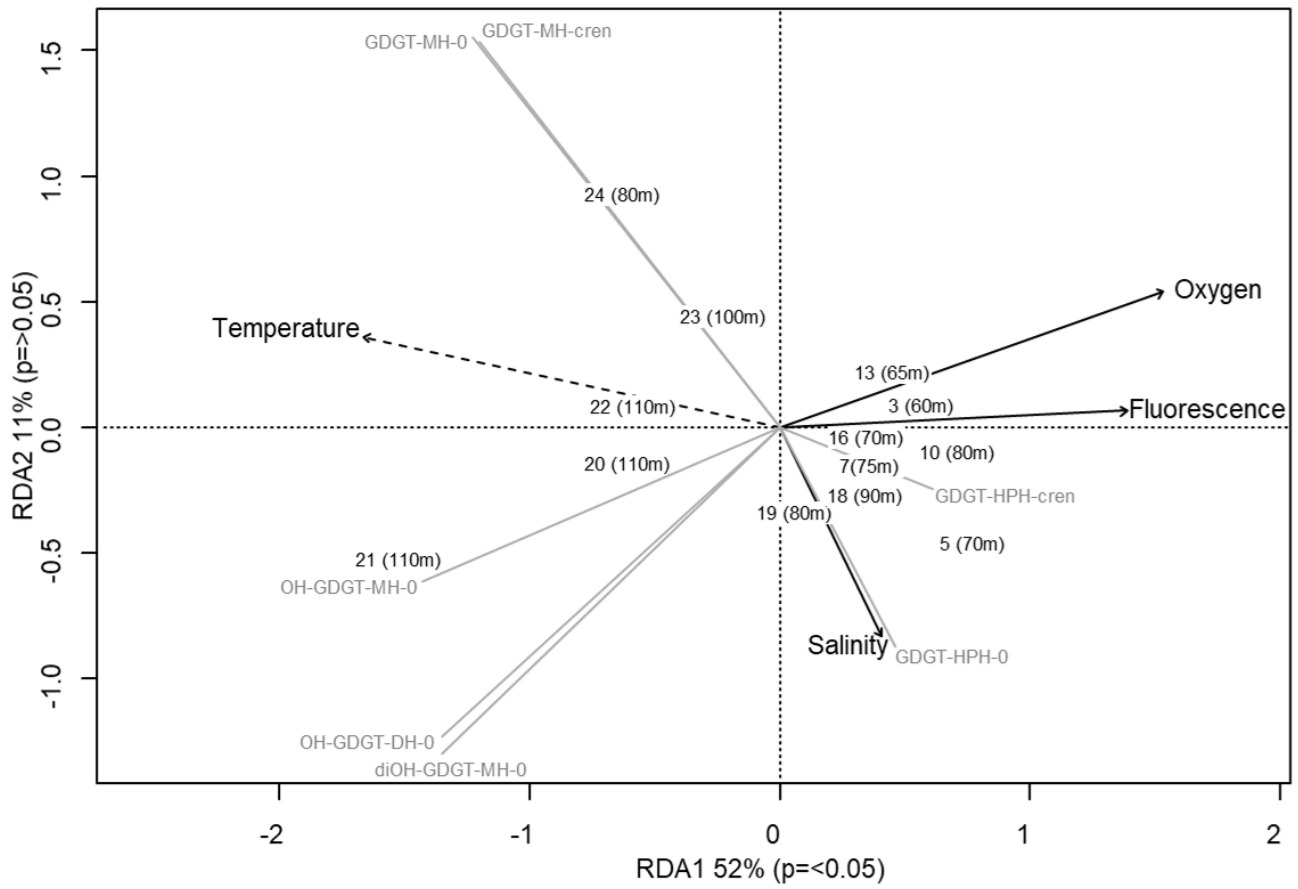
1023 Figure 4. Total IPL-GDGT concentration ( $\text{Log}_{10}$ , units/L) (A) and relative abundance (%) of IPL head  
 1024 groups, monohexose (MH, black), dihexose (DH, white), hexose-phosphohexose (HPH, grey) (B) in Scotia  
 1025 Sea thermocline samples (mixed layer samples excluded from plots).



1026

1027

1028 Figure 5. Redundancy analysis triplot for Scotia Sea sample set showing samples with depths, biomarker  
1029 response variables (grey lines), and explanatory variables (black with dashed lines indicating statistical  
1030 significance).



1031

1032 Supplement A. Absolute masses of IPLS detected in this study including for GDGTs, OH-GDGTs, and  
1033 diOH-GDGTs with either MH, DH, or HPH head groups, and for each adduct (H<sup>+</sup>, NH<sub>4</sub><sup>+</sup>, and Na<sup>+</sup>).

1034 Supplement B: S1. Intact GDGT structures showing GDGT cores where, GDGT: R & R' = H; OH-GDGT:  
1035 R=OH, R'=H; diOH-GDGT: R & R' = OH. Monohexose (MH), dihexose (DH), and hexose-phosphohexose  
1036 (HPH) polar head groups structures shown.

1037 S2. CTD matrix showing temperature (°C), salinity (PSU), chlorophyll fluorescence (mg/m<sup>3</sup>), dissolved  
1038 oxygen (μmol/kg) for CTD stations PS104/003 (A), PS104/007 (B), PS104/017 (C), PS104/022 (D),  
1039 PS104/043 (E), with seawater sample depths indicated by a triangle.

1040 Supplement C. Redundancy analysis output for Scotia Sea sample set including ANOVA.